HHS Public Access

Author manuscript

Sci Transl Med. Author manuscript; available in PMC 2022 September 16.

Published in final edited form as:

Sci Transl Med. 2022 March 16; 14(636): eabe8195. doi:10.1126/scitranslmed.abe8195.

Expression of the mono-ADP-ribosyltransferase ART1 by tumor cells mediates immune resistance in non-small cell lung cancer[++]

Erik Wennerberg[1,2,#], **Sumit Mukherjee**[3,4,#], **Sheila Spada**[1], **Clarey Hung**[3], **Christopher Agrusa**[3], **Chuang Chen**[3], **Amanda Valeta-Magara**[3], **Nils-Petter Rudqvist**[1], **Samantha Van Nest**[1], **Mohamed K. Kamel**[5], **Abu Nasar**[3], **Navneet Narula**[6], **Vivek Mittal**[3,7], **Geoff Markowitz**[3], **Xi Kathy Zhou**[8], **Prasad S. Adusumilli**[9], **Alain Borczuk**[10], **Thomas E. White**[11], **Abdul G. Khan**[11], **Paul Balderes**[11], **Ivo C. Lorenz**[11], **Nasser Altorki**[3], **Sandra Demaria**[1,10,*], **Timothy E. McGraw**[3,12,*], **Brendon M. Stiles**[3,4,*]

[1]Department of Radiation Oncology, Weill Cornell Medicine, New York, NY 10065, USA.

[2]Division of Radiotherapy and Imaging, The Institute of Cancer Research, London SM2 5NG, UK.

[3]Department of Cardiothoracic Surgery, Weill Cornell Medicine, New York, NY 10065, USA.

[4]Department of Cardiothoracic and Vascular Surgery, Albert Einstein College of Medicine, Bronx, NY 10461, USA

[5]Department of Surgery, Central Michigan University College of Medicine, Saginaw, MI 48602, USA.

[6]Department of Pathology, New York University, New York, NY 10016, USA.

[7]Department of Cell and Developmental Biology, Weill Cornell Medicine, New York, NY 10021, USA.

[8]Division of Biostatistics, Department of Population Health Sciences, Weill Cornell Medicine, New York, NY 10065, USA.

---

[*]Timothy McGraw, Department of Biochemistry, Weill Cornell Medicine, New York, NY 10065. temcgraw@med.cornell.edu. Phone: 212-746-4982. Sandra Demaria, Department of Radiation Oncology, Weill Cornell Medicine, New York, NY 10065, USA. szd3005@med.cornell.edu; Phone: 646-962-2092. Brendon Stiles, Department of Cardiothoracic and Vascular Surgery, Albert Einstein College of Medicine Montefiore Health System, Bronx, NY 10461, USA. brstiles@montefiore.org Phone: 718-920-5732.

Author contributions

BS, SD, TM, EW, and SM conceptualized and designed the study. EW, SM, SS, CH, CA, CC, AVM, and GM performed and analyzed and visualized in vitro and in vivo mouse experiments. CA, MKK, AN, NN, PA, AB, EW, and SM developed methodology, performed analysis, and performed validation of clinical samples. NR and SVN developed methodology and analyzed and visualized T cell RNA sequencing data.. BS, SD, TM, VM, and NA provided supervision and project administration. XKZ provided statistical support. TEW, AGK, ICL, and PB developed methodology, design, and testing of the ART1 blocking antibody. EW, SM, BS, SD, and TM wrote the initial draft and further edited and developed the manuscript. All authors have critically reviewed the manuscript.

[#]These authors contributed equally to this work

Supplementary Materials

Fig. S1 to S8

Table S1 to S4

MDAR Reproducibility Checklist

[9]Department of Surgery, Division of Thoracic Surgery, Memorial Sloan-Kettering Cancer Center, New York, NY 10065, USA.

[10]Department of Pathology and Laboratory Medicine, Weill Cornell Medicine, New York, NY 10021, USA.

[11]Tri-Institutional Therapeutics Discovery Institute, New York, NY 10021, USA.

[12]Department of Biochemistry, Weill Cornell Medicine, New York, NY 10065, USA.

Abstract

A majority of patients with non-small-cell lung cancer (NSCLC) do not achieve durable clinical responses from immune checkpoint inhibitors, suggesting the existence of additional resistance mechanisms. NAD-induced cell death (NICD) of P2X7-receptor (P2X7R)-expressing T cells regulates immune homeostasis in inflamed tissues. This process is mediated by mono-ADP-ribosyltransferases (ARTs). We found an association between membranous expression of ART1 on tumor cells and reduced CD8 T cell infiltration. Specifically, we observed a reduction in the $P2X7R^+$ CD8 T cell subset in human lung adenocarcinomas. In vitro, $P2X7R^+$ CD8 T cells were susceptible to ART1-mediated ADP-ribosylation and NICD, which was exacerbated upon blockade of the NAD^+-degrading ADP-ribosyl cyclase CD38. Finally, in murine NSCLC and melanoma models, we demonstrate that genetic and antibody-mediated ART1 inhibition slowed tumor growth in a CD8 T cell-dependent manner. This was associated with increased infiltration of activated $P2X7R^+$CD8 T cells into tumors. In conclusion, we describe ART1-mediated NICD as a mechanism of immune resistance in NSCLC and provide pre-clinical evidence that antibody-mediated targeting of ART1 can improve tumor control, supporting pursuit of this approach in clinical studies.

One Sentence Summary:

Tumor cell-expressed ART1 eliminates CD8 T cells through NAD-induced cell death, driving immune escape in lung cancer.

Introduction

Immune checkpoint inhibitors (ICI), alone or in combination with chemotherapy, have become the standard of care in patients with advanced non-small cell lung cancer (NSCLC) without targetable molecular alterations (1, 2). However, the majority of patients with lung cancer either do not respond to, or do not experience long-term benefit from, ICI (3, 4). Thus, there is an urgent need to identify other robust biomarkers predictive of response to ICI, and to understand the mechanisms of primary and acquired resistance of lung cancer to immunotherapy.

In humans, ADP-ribosyltransferase-1 (ART1) is expressed at low concentrations in healthy tissues including the lung (5). ART1 is a glycosylphosphatidylinositol (GPI)-anchored enzyme, with an extracellular catalytic domain. Therefore, ART1 can mono-ADP-ribosylate extracellular proteins in the local microenvironment, altering their function (5–7). The expression of ART1 in lung cancer has not been investigated, but previous studies have

suggested increased ART1 protein expression in colorectal cancer and in glioblastoma, where high expression was associated with a poor prognosis (8). In mouse models of colorectal cancer, ART1 expression was shown to promote a more aggressive phenotype with increased epithelial-to-mesenchymal transition, cellular proliferative signaling, and increased angiogenesis (9, 10). However, it has not been determined whether tumor ART1 expression could regulate tumor crosstalk with the immune microenvironment.

Among the well described targets of ADP-ribosyl transferases is the P2X7 receptor (P2X7R, gene id: *P2RX7*). P2X7R is an ATP-gated cation channel of the purinergic type 2 receptor family, with low affinity for extracellular ATP, that activates pro-inflammatory pathways (11). It is expressed on multiple immune cell subsets, including T cells, and its expression is essential for inflammatory responses and anti-tumor immunity (12, 13). P2X7R can also be overexpressed on cancer cells where it may promote tumor progression (14). However, in NSCLC, high P2X7R expression has been associated with improved overall and progression-free survival (15). In pathological conditions, such as tissue damage, inflammation, or tumor development, cytosolic NAD^+ is released into the local extracellular environment where it may be used as a substrate by extracellular ADP-ribosyl transferases to catalyze the transfer of the ADP-ribose to P2X7R (13). This covalent modification results in constitutive activation of P2X7R, triggering large pore formation, uncontrolled calcium influx and phosphatidylserine externalization. This leads to a process known as NAD-induced cell death (NICD) (16). Typically, extracellular NAD^+ concentrations are low and tightly regulated by the ADP-ribosyl cyclase CD38, which is expressed on activated immune cells, as well as on cancer cells (17, 18). However, even in the presence of CD38, extracellular NAD^+ concentrations can increase following rapid release from stressed or dying cells (13). In preclinical studies, ART-mediated NICD of T cells has been proposed as a homeostatic mechanism to eliminate naïve and bystander T cells in inflamed tissues (19). More recently, NICD was shown to regulate the homeostasis of CD4 regulatory T (CD4 T_{reg}) cells which have broad immunoregulatory function, but also of tissue-resident memory T (T_{RM}) cells, the presence of which in lung tumors has been associated with good prognosis (20–22). These pre-clinical studies focused on the role of ADP-ribosyltransferase-2 (ART2) in immune modulation through NICD. ART2 is expressed on murine lymphocytes where it can auto-ADP-ribosylate P2X7R, mediating NICD in cis. However, in humans, the ART2 gene contains premature stop codons, rendering it a pseudogene, whereas other ART family members such as ART1, ART3, ART4 and ART5 are transcriptionally active (23).

In the current study, we show that ART1 is expressed on the surface of human lung cancer cells and that its expression is associated with reduced lung tumor infiltration of $P2X7R^+$ CD8 T cells. In preclinical models of lung cancer and melanoma, ART1 expression on tumor cells promoted escape from CD8 T cell-mediated tumor control. ART1-blockade with a therapeutic monoclonal antibody reduced the growth and dissemination of ART1-expressing tumors in immunocompetent mice and promoted tumor infiltration of activated $P2X7R^+$ CD8 T cells. Overall, our data suggest that ART1 tumor expression is a mechanism of immune resistance and that ART1 is an actionable target to enhance T cell-mediated tumor rejection.

Results

ART1 is expressed in human NSCLC and is associated with reduced CD8 T cell infiltration.

ART1 expression was assessed in human NSCLC lines A549 and H1650 and in a benign bronchial epithelial cell line (BEAS2B) by immunofluorescence. The tumor cell lines had heterogeneous expression of cell surface (Fig. 1A and B) and total cell ART1 (Fig. 1A, fig. S1A). Both tumor cell lines had higher ratios of cell surface:total cell expression than did BEAS2B cells (59.5% and 55.4% versus 29.2% respectively, Fig. 1C). We next sought to evaluate ART1 expression in human lung tumors. Analysis of ART1 gene expression by real time quantitative polymerase chain reaction (RT-qPCR) in tumor and matched normal lung tissue from 40 patients with stage I to III lung adenocarcinoma showed higher mean expression in the cancer samples, driven by a fraction of the tumors with markedly higher expression (Fig. 1D). Of note, the matched tumors also had lower expression of glycosylphosphatidylinositol specific phospholipase D1 (GPLD1), the only well-characterized mammalian phospholipase regulating cleavage of GPI anchors (fig. S1B). Cell-associated GPLD1 can release GPI-anchored proteins from the cell surface, but expression has been shown to be down-regulated with stress in lung cancer cells, suggesting that tumor cells are more likely to retain ART1 on the cell surface than benign cells (24).

To determine ART1 protein expression, a tissue microarray of 493 treatment-naïve stage I lung adenocarcinomas was analyzed for ART1 expression by immunohistochemistry (25). Staining for ART1 in the cancer cells was strong, moderate, and weak in 55%, 42% and 3% of the tumors, respectively (fig. S1C and table S1). For the most part, ART1 expression by immunohistochemistry) in the cancer cells was diffuse cytoplasmic; however, staining concentrated near the cell periphery and plasma membrane (“membranous”) was identified in 10% of the tumors (Fig. 1E and table S2). Tumors with a mucinous histologic subtype, a rare tumor which only comprised 3.7% of the cohort, were particularly likely to express membranous ART1 compared to other histologic subtypes (44% versus 8.4%). Tumors were also scored for infiltration of CD3-, CD8-, CD4-, and FoxP3-expressing T cells, CD20-expressing B cells, CD56-expressing natural killer (NK) cells, and CD68- or CD163-expressing macrophages (table S3). There was no correlation between overall ART1 staining intensity and immune cell infiltration (table S1). However, tumors with membranous ART1 staining were more likely to have low CD8 T cell infiltration as compared to tumors with only diffuse cytoplasmic ART1 (72% versus 44%, Fig. 1F, table S2).

Next, we analyzed transcriptomic data from a lung adenocarcinoma cohort (TCGA, PanCancer Atlas) using the cBioportal platform to assess whether ART1 tumor expression was associated with differential expression of genes associated with CD8 T cell cytotoxicity, such as interferon (IFN)-γ (*IFNG*), Granzyme A (*GZMA*), Granzyme B (*GZMB*), Perforin 1 (*PRF1*), 41BB (*TNFRSF9*), as well as genes associated with immunoregulation, such as cytotoxic T lymphocyte antigen-4 (CTLA-4, encoded by *CTLA4*), programmed cell death-1 (PD-1, encoded by *PDCD1*), T cell immunoglobulin and mucin-domain containing-3 (Tim-3, encoded by *HAVCR2*), lymphocyte activation gene-3 (Lag-3, encoded by *LAG3*) and T cell immunoglobulin and ITIM domain (Tigit, encoded by *TIGIT*). We generated a heatmap using cBioportal’s OncoPrint with clustering, which showed that high ART1

mRNA expression was associated with low expression of CD8 T cell cytotoxicity genes and immunoregulatory genes (Fig. 1G).

ART1 tumor expression increased immune resistance in mouse lung tumor models.

To test the hypothesis that ART1 expression protects tumors from T cell-mediated rejection, we developed a mouse model of ART1 over-expressing NSCLC. We introduced an ART1 plasmid into KP1 cells, which were originally derived from inducible $KRAS^{G12D/+}/p53^{-/-}$ mice (KP1 $ART1^{OE}$) (26). The parent wild type KP1 line had low ART1 cell surface expression at baseline, whereas the engineered KP1 $ART1^{OE}$ line showed an approximately 9-fold increase in ART1 surface expression per cell by immunofluorescence (fig. S2A). In order to modulate ART1 expression, KP1 $ART1^{OE}$ cells were transduced with a doxycycline-inducible short hairpin RNA (shRNA) targeting ART1 (shART1) (26). Doxycycline-induced ART1-knockdown markedly reduced both ART1 cell surface expression (fig. S2A) and ADP-ribosylation of tumor cell surface targets on the cancer cells themselves (fig. S2B). Proliferation of KP1 $ART1^{OE}$ cells remained unaffected by ART1 knockdown (fig. S2C).

To test the effect of ART1 expression on tumor growth in vivo, KP1 $ART1^{OE}$ cells were subcutaneously inoculated in immunocompetent wild type and T cell-deficient nude C57BL/6 mice. Half of the mice in each group were given doxycycline to induce ART1 knockdown in vivo, which was confirmed by immunofluorescence staining of tumor specimens (fig. S2D). In immunocompetent mice, KP1 $ART1^{OE}$ flank tumors grew rapidly, whereas doxycycline-induced ART1 knockdown delayed flank tumor growth (Fig. 2A, left panel). In T cell-deficient nude mice, KP1 $ART1^{OE}$ flank tumors had a similar growth rate as in wild type mice. However, the effect of ART1 knockdown on tumor growth was abrogated only in immunocompetent mice, suggesting that the tumor-promoting effects of ART1 might be T cell-dependent (Fig. 2A, right panel). Next, we sought to test the role of ART1 overexpression in an orthotopic lung tumor model. To generate KP1 $ART1^{OE}$ lung tumors, KP1 $ART1^{OE}$ cells were injected in the tail vein, and cohorts of the mice were given doxycycline to induce ART1 knockdown in vivo (Fig. 2B). ART1 knockdown resulted in a decreased lung tumor burden at day 14, as assessed by counting the number of tumors in hematoxylin and eosin (H&E) stained lung sections (Fig. 2C). Lung CD8 T cell infiltration was determined by flow cytometry at days 16 and 25. At day 25 after tumor injection, mice with induced ART1 knockdown had higher frequency of CD8 T cells among total lung tumor-infiltrating leukocytes ($CD45^+$ cells) than mice bearing ART1-expressing tumors (Fig. 2D). The percentage of tumor-infiltrating CD8 T cells was decreased at day 25 compared to day 16 in control mice, consistent with a loss of immune control associated with tumor progression (Fig. 2D).

To test the role of ART1 in tumor progression in a second immunocompetent mouse tumor model, we chose a melanoma line, as human melanomas are shown to strongly express ART1 in the Human Protein Atlas. B16-F10 mouse melanoma cells have high intrinsic ART1 cell surface expression and we generated an ART1-negative derivative using clustered regularly interspaced palindromic repeats (CRISPR)/ CRISPR associated protein 9 (Cas9) and two different guide RNA (fig. S3A and B). We observed that subcutaneous injection

of control B16-F10 cells in syngeneic immune competent mice resulted in formation of rapidly growing flank tumors, whereas ART1-deficient B16-F10 cells showed markedly impaired tumor growth or failed to form palpable tumors (fig. S3C). The impaired growth of ART1-deficient B16-F10 cells in vivo was not due to decreased fitness of the cancer cells themselves since, in vitro, ART1-deficient cells proliferated faster than ART1-expressing B16-F10 cells (fig. S3D).

Development of an inhibitory ART1 antibody.

Next, we explored therapeutic targeting of surface ART1 using a monoclonal antibody targeting ART1. Therapeutic antibody candidates were initially developed through immunization of AlivaMab Mouse transgenic mice with a human immunoglobulin repertoire utilizing recombinant human ART1 protein. Candidate antibodies that bound to both human and mouse ART1 and inhibited mono-ADP-ribosylation were further developed (fig. S4A and B). The lead candidate, 22C12, which potently inhibited ART1 enzymatic activity in the primary screening assay, contained a human variable heavy chain and a mouse variable kappa light chain, which was used for in vivo and mechanistic studies. Later in the project, we were able to generate a fully humanized 22C12 antibody with a human light chain (22C12 (HuLC)) which was tested together with the original 22C12 antibody to confirm binding and inhibitory activity in vitro. Binding of 22C12 antibodies to HEK 293 cells transfected with ART1 (HEK-ART1^{OE}) was determined by flow cytometry showing half-maximum binding (EC_{50}) values in the range of 0.8–1.5 nM (fig. S4C). Half-maximum inhibition of ADP-ribosylation (IC_{50}), by 22C12 antibodies, as determined by cell surface ADP-ribosylation of HEK-ART1^{OE} cells, was achieved at 4.5 nM antibody concentration for both 22C12 and 22C12 (HuLC) (fig. S4D). Binding of 22C12 to KP1 ART1^{OE} cells was assessed by flow cytometry staining (fig. S4E) and the ability of 22C12 to block cancer cell induced mono-ADP-ribosylation was confirmed in KP1 ART1^{OE} cells co-cultured with NAD^+ (fig. S4F). We assessed potential toxicity of systemic administration of 22C12 antibodies in tumor-naïve mice by intraperitoneal (i.p.) injections of 25 mg/kg every three days for three weeks and monitored for weight loss and blood glucose concentrations at baseline and every week until the end of the study. The mice remained normal in appearance, activity, gait, and alertness throughout the study (fig. S4G and H).

ART1 blockade reduces lung tumor burden and promotes infiltration of P2X7R$^+$ CD8 T cells

To test the in vivo anti-tumor activity of 22C12, intratumoral injections of the 22C12 antibody or an isotype subclass-matched control antibody (5 mg/kg) were performed on subcutaneously implanted KP1 ART1^{OE} flank tumors (fig. S5A to C). ART1 blockade resulted in delayed tumor growth compared to tumors treated with isotype control antibody (fig. S5B), with average tumor weight at day 25 lower in the mice treated with 22C12 compared with isotype control antibody (fig. S5C). Next, we assessed the anti-tumor effect and immunomodulatory properties of systemic ART1 blockade in the orthotopic KP1 ART1^{OE} lung tumor model. Mice were treated i.p. with 22C12 antibody (25 mg/kg) or the equivalent dose of isotype control antibody starting on day 6 after tumor cell injection until day 18 (Fig. 3A). On day 19, mouse lungs were isolated, fixed, and stained with H&E to assess lung tumor burden, which showed fewer and smaller tumor nodules in mice treated

with 22C12 antibody compared with isotype-treated mice (Fig. 3B to D). To confirm our observations in a second lung tumor model we first assessed endogenous surface ART1 expression on Lewis lung carcinoma (LLC1) cells and found them to express more ART1 than KP1 wild type cells, but less than KP1 ART1^{OE} cells (fig. S2A). In an LLC1 orthotopic lung tumor model (treatment strategy as in Fig. 3A), mice treated with ART1 blockade had reduced lung tumor burden compared to mice treated with control antibody (fig. S5D and E).

Next, we performed flow cytometry analysis on digested KP1 ART1^{OE} tumor-bearing lungs to assess how ART1 blockade affects P2X7R expression in the CD8 T cell compartment. We also assessed expression of Ki67 expression indicating the state of proliferation and expression of the immunoregulatory receptor PD-1 indicating activation and tumor-engagement (27). Considering recent studies showing a susceptibility of P2X7R$^+$ T_{RM} cells to NICD (20), we assessed whether ART1 blockade increased the infiltration of P2X7R$^+$ memory CD8 T cell subsets including central memory (T_{CM}, CD62L$^+$CD44$^+$CD69$^-$), effector memory (T_{EM}, CD62L$^-$CD44$^+$CD69$^-$), and T_{RM} (CD62L$^-$CD44$^+$CD69$^+$) CD8 T cells. The majority of P2X7R$^+$ CD8 T cells co-expressed Ki67, indicating that they were in a proliferative state, and we observed that ART1-blockade increased the percentage of P2X7R$^+$Ki67$^+$ but not of the P2X7R$^-$Ki67$^-$ CD8 T cell subset (Fig. 3E). PD-1 was co-expressed on a subset of P2X7R$^+$ CD8 T cells and we observed an increase in the percentage of PD-1 expression both in the P2X7R$^-$ and P2X7R$^+$ CD8 T cell subset following ART1 blockade (Fig. 3F). Further, we found that absolute numbers of CD8 T cells expressing P2X7R and Ki67 normalized to lung tissue weight were elevated in mice treated with ART1 blockade compared to control mice (Fig. 3G). ART1 blockade increased the infiltration of P2X7R$^+$ T_{RM} cells, whereas P2X7R$^+$ T_{EM} and T_{CM} cell populations were not increased (Fig. 3H). Enrichment of P2X7R$^+$ CD8 T cells, was also observed following ART1 blockade in the LLC1 lung tumor model (fig. S5F) and following ART1 knockdown in the KP1 ART1^{OE} orthotopic lung tumor model, (fig. S5G).

Our findings indicated that tumor ART1 expression modulates intratumoral CD8 T cells. To determine the role of T cells on the therapeutic effect of ART1 blockade, CD8 and CD4 T cell were depleted and mice with KP1ART1^{OE} orthotopic lung tumor were treated with systemic 22C12 antibody starting on day 6 after tumor cell injection (Fig. 3I). Lungs were harvested on day 19 after tumor cell injection to assess tumor burden by H&E staining. The number and size of lung tumor nodules was reduced in mice treated with ART1 blockade compared to mice treated with isotype control antibodies. This effect was largely abrogated by CD8, but not CD4, T cell depletion (Fig. 3J and K), suggesting that the majority of the effect of ART1 blockade is CD8 T cell-dependent.

Next, the role of CD8 and CD4 T cells in tumor control was tested in the B16-F10 model using genetic deletion of ART1 (fig. S6). CD8 and CD4 T cell depletion did not affect tumor control or survival of mice bearing ART1-expressing B16-F10 tumors (fig. S6A). In contrast, CD8 T cell depletion reduced the survival of mice bearing ART1-deficient B16-F10 tumors. CD4 T cell depletion did not have an effect on survival compared with isotype control treated animals (fig. S6B).

P2X7R$^+$ CD8 T cells are susceptible to ART1-mediated NICD.

Borges da Silva and colleagues have shown that P2X7R expression on CD8 T cells plays a role in establishing tissue residency, metabolic fitness, and survival (28, 29). However, in acutely inflamed tissues characterized by increased extracellular NAD^+, CD8 T cells expressing P2X7R are targets for ART-mediated NICD, as demonstrated by Stark *et al.* (19, 20). In light of our findings that tumor-infiltrating P2X7R$^+$ CD8 T cells co-expressed Ki-67 and PD-1 and that their infiltration in lung tumors increased upon ART1 blockade, we next investigated *P2RX7* expression of CD8 T cells over the course of lung tumor progression. RNA sequencing analysis on CD8 T cells isolated from lungs and spleens of mice orthotopically inoculated with wild type KP1 cells, which have low ART1 expression, on day 7 and 17 after tumor inoculation showed that *P2RX7* expression was increased at day 17 compared with CD8 T cells isolated from lungs of naïve mice. CD8 T cells from tumor-bearing mice also co-expressed *IFNG*, *PRF1*, *PDCD1*, *CTLA4*, *HAVCR2*, *LAG3*, and *TIGIT* (fig. S7A). Furthermore, observed changes in *P2RX7* expression were confined to the lung tumor-resident CD8 T cells, as we did not observe similar expression changes in spleen-derived CD8 T cells (fig. S7A and B). We confirmed by flow cytometry that surface expression of P2X7R on CD8 T cells from mice with high KP1 lung tumor burden was elevated compared to CD8 T cells from lungs of naïve non-tumor-bearing mice (fig. S7C).

We next sought to specifically assess whether P2X7R is a target for ART1-mediated ADP-ribosylation and NICD of lung-tumor infiltrating T cells. To this end, after confirming by quantitative (q)PCR that neither CD8 or CD4 T cells express ART1 (fig. S7D), we established an in vitro assay where T cells isolated from lungs of wild type KP1 tumor-bearing mice were incubated with or without enzymatically active recombinant murine ART1 (rART1) (fig. S8A). ADP-ribosylation was detected using etheno-tagged NAD^+ (eNAD) (30), and DAPI was used to measure cell death. In order to assess whether expression of CD38 could play a cytoprotective role by catabolizing free NAD^+ from the immediate micromilieu, a CD38-blocking antibody was added to selected cultures (18).

Since ART2 is expressed on murine lymphocytes and can mediate auto-ADP-ribosylation of T cells in cis, we used an ART2-blocking nanobody (s+16a) to block its activity, as reported by Koch-Nolte and colleagues (19, 31). ART1 was blocked using 22C12 antibody. We confirmed the ability of ART2 blocking nanobodies and ART1 blocking antibodies to inhibit ADP-ribosylation in an experiment where T cells were cultured in the presence of eNAD alone. ART2 blockade resulted in reduced ADP-ribosylation of CD8 T cells from 70.1± 8.8% to 12.9±2.6% and of CD4 T cells from 54.6±9.6% to 9.3±7.2%. ART1-blockade did not affect ADP-ribosylation of CD8 or CD4 T cells (fig. S8B).

Considering previous studies which show a susceptibility of CD4$^+$ T_{reg} cells to NICD through P2X7R (22), we separately analyzed ADP-ribosylation and NICD on CD4 T_{reg} cells, CD4 conventional T (T_{conv}) cells and CD8 T cells as well as on P2X7R$^+$ and P2X7R$^-$ fractions of the T cell subsets separately (Fig. 4A). Average P2X7R expression was 9.3±2.4% of CD8 T cells, 21.6±3.9% of CD4 T_{conv} cells and 80.8±2.6% of CD4 T_{reg} cells. ADP-ribosylation was measured by the frequency of cells that stained positive for eNAD (Fig. 4B) and NICD was measured by the frequency of cells that stained positive for both eNAD and DAPI (Fig. 4C). We found that P2X7R$^+$, but not P2X7R$^-$, CD8 T cells were

sensitive to ART1-mediated ADP-ribosylation and ICD which was increased in the presence of CD38 blocking antibodies. CD4 T_{conv} cells had a low degree of ADP-ribosylation in the presence of rART1, regardless of P2X7R expression, but CD38-blockade markedly increased ADP-ribosylation. However, ART1-mediated NICD of CD4 T_{conv} cells remained low even with CD38 blockade. We observed ART1-mediated ADP-ribosylation and NICD of both $P2X7R^-$ and $P2X7R^+$ CD4 T_{reg} cells. However, in contrast to its effect on $P2X7R^+$ CD8 T cells, CD38 blockade did not increase ADP-ribosylation of $P2X7R^+$ CD4 T_{reg} cells but instead reduced ART1-mediated NICD of this subset. ART1 blockade reduced ART1-mediated ADP-ribosylation and NICD of CD8 T cells as well as CD4 T_{conv} and CD4 T_{reg} cells to baseline values (Fig. 4B and C)

Together, these data indicate that CD8 T cells and CD4 T_{reg} cells are susceptible to ART1-mediated ADP-ribosylation and NICD through P2X7R. We hypothesized that the difference in susceptibility of $P2X7R^+$ CD8 T cells and $P2X7R^+$ CD4 T_{conv} cells to ART1-mediated NICD, could be explained by a difference in their relative expression of the *P2RX7* splice variants *P2RX7-a* and *P2RX7-k*, the latter of which has been shown to be more prone to trigger NICD when ADP-ribosylated compared with the *P2RX7-a* variant (32). As suggested by previous studies, tumor cells are also known to express P2X7R which could render them susceptible to ART1-mediated NICD (12). Therefore, KP1, B16, and LLC1 tumor cell lines were analyzed for expression of the *P2RX7* splice variants alongside CD8 T cells and CD4 T_{conv} cells isolated from KP1 tumor-bearing lungs. CD8 T cells and CD4 T_{conv} cells comparably expressed *P2RX7-k*, whereas KP1, LLC1 and B16 tumor cells expressed low concentrations of *P2RX7-k* (fig. S8C). *P2RX7-a* expression was low in both CD8 T cells and CD4 T_{conv} cells; in contrast, we detected higher expression in KP1, LLC1 and B16 cells, which may protect ART1-expressing tumor cells from NICD following auto-ADP-ribosylation (fig. S8D). In line with these findings, proliferation assays demonstrate that ART1-expressing tumor cells grown in the presence of NAD^+ or ART1 blockade had no differences in cell growth (fig. S8E to G).

ART1-expressing human lung tumors have reduced infiltration of $P2X7R^+$ CD8 T cells.

We next sought to determine whether infiltration of $P2X7R^+$CD8 T cells is modulated in human lung tumors and whether it is associated with ART1 expression. Matched lung tumor and adjacent normal tissue from twelve patients with lung adenocarcinoma treated with surgery were stained for ART1 expression. We observed a heterogeneous expression of ART1 in both lung tumor tissue and normal tissue. However, ART1 expression was higher in lung tumor tissue compared to normal tissue, as measured by fluorescence intensity of the immunostained sections (Fig. 5A and B). Further, the average percentage of $P2X7R^+$ CD8 T cells among total CD8 T cells was lower in lung tumor tissue compared with normal tissue (Fig. 5C and D). A linear regression analysis of all samples showed that the frequency of $P2X7R^+$ CD8 T cells was inversely correlated with tissue ART1 mean fluorescence intensity (MFI) (Fig. 5E). We next plotted the percent increase of $P2X7R^+$ CD8 T cells from normal tissue to lung tumor tissue against the fold increase in ART1 MFI from normal to lung tumor tissue which showed a strong inverse correlation (Fig. 5F) Further, we performed flow cytometry analysis on dissociated tissue from five patients with lung adenocarcinoma to quantify expression of P2X7R and CD38 on CD8 T cells.

The percentage of P2X7R$^+$CD8 T cells among total CD8 T cells was lower in the lung tumor compared to normal tissue (Fig. 5G and H). We observed that tumor-infiltrating P2X7R$^+$CD8 T cells expressed high concentrations of CD38 which was elevated compared to normal tissue (Fig. 5G and I). These data indicate that expression of ART1 in human lung cancer, similarly to the mouse models, is associated with decreased tumor infiltration by P2X7R$^+$ CD8 T cells that co-express CD38, suggesting that the latter may have a protective role against ART1-mediated NICD in the tumor microenvironment.

Discussion

The tumor immune contexture is associated with prognosis and response to immunotherapy, with CD8 T cell infiltration generally serving as an indicator of an ongoing anti-tumor immune response which can be reinvigorated by ICI (33, 34). To improve patient outcomes, it is critical to gain an improved understanding of the factors that regulate CD8 T cell infiltration and their function in the tumor. In normal tissue, ART-mediated ADP-ribosylation and NICD regulate T cell homeostasis following tissue damage or infection (19, 20, 28). However, whether this mechanism is involved in the regulation of CD8 T cell infiltration within tumors, and whether expression of ARTs is dysregulated in human cancer, has not been previously investigated. In the present study, we show that ART1 overexpression on human lung cancer cells is associated with reduced intratumoral CD8 T cells, specifically a reduction in the P2X7R$^+$ CD8 T cell subset. Furthermore, we demonstrate that expression of ART1 in mouse tumors promotes tumor growth in immune competent but not in T cell-deficient mice or following CD8 T cell depletion, and that ART1 expression is associated with a reduction in tumor-infiltrating P2X7R$^+$CD8 T cells. In vitro, P2X7R$^+$, but not P2X7R$^-$, CD8 T cells were susceptible to ART1-mediated ADP-ribosylation and to NICD, which was exacerbated upon blockade of CD38. Overall, these data identify ART1 expression in lung cancer, and possibly in other cancers, as a regulator of CD8 T cell infiltration in the tumor microenvironment. As such, we consider ART1 to be a potential actionable target to improve immune-mediated tumor control. As an extracellular, membrane-anchored enzyme, ART1 should be highly druggable. Here, we demonstrate that treatment with a monoclonal antibody that binds to and inhibits ART1-induced ADP-ribosylation had therapeutic benefits in preclinical models, resulting in reduced growth of ART1$^+$ lung cancer and increased tumor-infiltration of activated proliferating, and T_{RM} P2X7R$^+$ CD8 T cells.

Despite an expanding knowledge of the role of mono-ADP-ribosylation in tumor development, ART1 has only recently been described to play a role in cancer progression. In a model of mouse colon adenocarcinoma, Xu *et al.* demonstrated that overexpression of ART1 facilitated tumor growth, whereas knockdown inhibited tumor growth in various immune competent models (35). This effect was attributed to cis-ADP-ribosylation of integrin and Rho effector family members, subsequently affecting downstream mediators of cellular migration. Although we have not investigated this pathway, our observations show that the anti-tumor effects of ART1 knockdown or blockade in mouse lung cancer models is dependent on CD8 T cells. In vitro, knockdown of ART1 had no effect on KP1 ART1^{OE} cell proliferation and actually enhanced tumor cell proliferation of B16-F10 mouse melanoma cells yet resulted in impaired tumor growth in vivo in immunocompetent mice.

Thus, although ART1 has cancer cell-intrinsic effects that may be model-dependent, the immune suppressive effects of ART1 expression dominate in our in vivo models.

We demonstrate here that these effects are predominantly mediated through mono-ADP-ribosylation of P2X7R on CD8 T cells. Preclinical studies have painted a complex picture of the role of P2X7R in tumor progression and anti-tumor immunity. Di Virgilio and colleagues demonstrated increased tumor progression associated with low CD8 T cell infiltration in P2X7R-deficient mice in the B16-F10 melanoma model (12). In contrast, administration of a P2X7R antagonist to wild type mice bearing B16-F10 tumors resulted in reduced tumor growth and increased immune activation (36). These seemingly contradictory results can be explained by the fact that P2X7R is required for the activation of the inflammasome in dendritic cells by ATP released by dying cancer cells, which was required for priming of anti-tumor CD8 T cells (37). Thus, in P2X7R-deficient mice, there is a failure to initiate the anti-tumor immune response. In contrast, pharmacological inhibition of P2X7R after CD8 T cell priming has already occurred may prevent NICD of $P2X7R^+$ CD8 T cells induced by ART1, which we show here to be highly expressed in B16-F10 melanoma cells. Here, we demonstrate that, ART1 knockdown in B16-F10 tumors reduces tumor progression in a CD8 T cell-dependent manner. Further, we show, in two lung tumor models, that ART1 blockade in immunocompetent mice with established tumors promotes $P2X7R^+$ CD8 T cell infiltration and reduces tumor burden.

Our mechanistic studies showed that $P2X7R^+$ CD8 T cells, and to a lesser extent CD4 T_{reg} cells, are susceptible to ART1-mediated NICD through P2X7R. The lack of susceptibility of $P2X7R^+$ CD4 T_{conv} cells to ART1-mediated NICD is intriguing. We hypothesized that selective gene expression of the *P2RX7-a* splice variant, which is less prone to trigger NICD, may explain this disparity. However, we did not detect high abundance of this variant in either CD4 T_{conv} or CD8 T cells isolated from tumor-bearing lungs, indicating that there may be other cell-intrinsic mechanisms at work that render $P2X7R^+$ CD8 T cells uniquely sensitive to ART1-mediated NICD. However, our finding that tumor cells predominantly express *P2RX7-a* may indicate a mechanism by which tumor cells that co-express ART1 and P2X7R can avoid triggering auto-ADP-ribosylation and NICD.

Recent studies have shown that P2X7R expression in recirculating memory CD8 T cells is essential for extracellular ATP-driven maintenance of mitochondrial function and metabolic fitness (28), that generation of CD8 T_{RM} cells through transforming growth factor (TGF)-β sensing is dependent on P2X7R (29) and that T_{RM} cell homeostasis is regulated by NICD through P2X7R (20). In line with these findings, we found that ART1 blockade increases infiltration of $P2X7R^+$ CD8 T_{RM} cells in tumor-bearing lungs. Together with our observation that lung tumor-infiltrating CD8 T cells have elevated expression of P2X7R and co-express cytotoxic and immunoregulatory markers, we postulate that $P2X7R^+$ CD8 T cells infiltrating lung tumors represent a critical tissue-resident subset of memory T cells with anti-tumor activity. P2X7R expression in patients with NSCLC has been associated with improved survival (15). However, in patients with high ART1 tumor expression, the anti-tumor effect of $P2X7R^+$ CD8 T cells may be abrogated due to ART1-mediated NICD.

T cell expression of CD38 may also be a critical component in determining whether cells undergo NICD. CD38 is upregulated on mouse and human T cells upon activation and differentiation (17) and may represent a cytoprotective mechanism to avoid ADP-ribosylation and NICD in NAD^+ enriched inflamed tissues (19). Our results indicate that CD38 blockade enhances ADP-ribosylation and NICD of $P2X7R^+$ CD8 T cells in the presence of ART1. In addition, we found that a subset of $CD38^+$ $P2X7R^+$ CD8 T cells were enriched in $ART1^+$ human lung tumors, suggesting that CD38 expression may enable survival of a subset of anti-tumor CD8 T cells that would have otherwise been eliminated by ART1-mediated NICD through P2X7R. Importantly, our in vitro experiments show that ART1-mediated NICD of $P2X7R^+$ CD4 T_{reg} cells was abrogated following CD38 blockade. Hence, in a clinical setting, treatment of patients with ART1-positive adenocarcinoma with CD38 blockade could have the dual detrimental effect of exacerbating NICD of CD8 T cells while protecting CD4 T_{reg} cells, thus skewing the CD8 T cell to CD4 T_{reg} cell ratio, which is associated with immunotherapy response and tumor rejection (38).

Our findings have potential implications for the design of clinical studies targeting CD38 to enhance anti-tumor immunity. In addition to T cells, CD38 is expressed by other immune cells and some cancer cells and has been shown in pre-clinical studies to contribute to acquired resistance to PD-1 or programmed death-ligand 1 (PD-L1) blockade by converting NAD^+ into ADP-ribose (ADPR), a precursor of adenosine, which has broad immune suppressive function (18). The anti-CD38 antibody daratumumab was recently tested in combination with atezolizumab (an anti-PD-L1 antibody) in patients with NSCLC in a clinical trial (NCT03023423). This study was terminated early because of increased mortality in the combination treatment arm. Although the reasons for this outcome are unclear, it is intriguing to consider whether increased NICD of anti-tumor T cells could have contributed. ART1 expression has been demonstrated to increase following cellular stress (39), so we anticipate that its expression in tumors may be highly dynamic and potentially fluctuate depending on the degree of inflammation in the TME as well as in response to treatment. Hence, the immunomodulatory effects of ART1 may play an even more substantial role following treatment with cytotoxic agents such as chemotherapy and radiation. Such treatments will also contribute to increased concentrations of extracellular NAD^+ following cell death, potentially priming the local microenvironment for ART1-induced NICD. Thus, more studies into the role of ART1 as an actionable barrier to response to combinations of cytotoxic agents or radiotherapy with immunotherapy are needed.

Our study has several limitations. ART1-mediated ADP-ribosylation might have tumor-promoting effects other than NICD, the focus of this study. Consequently, these other possible effects cannot be discounted when considering the impact of our pre-clinical findings on understanding the full contribution of ART1 on immunomodulation and tumor progression in patients with cancer. Additionally, other immune cell types in the tumor microenvironment may be targets of ART1-mediated NICD, the validation of which requires further investigation. In this regard, expanding the correlation of ART1 expression to tumor CD8 T cell infiltration to a larger patient cohort will strengthen our proposal that CD8 T cells are a primary target of ART1 for immune escape in NSCLC. Further, ART1's role in immune escape in other cancers also needs to be analyzed to assess if ART1 blockade may be a general cancer immunotherapeutic strategy.

In conclusion, we describe an immune resistance mechanism in NSCLC by which ART1-expressing tumor cells eliminate tumor-infiltrating CD8 T cells by NICD. Our findings suggest that ART1 tumor expression may have prognostic and predictive value in patients with lung cancer undergoing immunotherapy. Pharmacologic targeting of ART1 holds promise to potentiate CD8 T cell-mediated immune responses in patients with NSCLC. Further studies on combinations of ART1 blockade and ICI are warranted.

Materials and Methods:

Study Design

The objectives of our study were (1) to determine whether ART1 expression in human NSCLC tumors regulates immune cell infiltration, (2) to assess in mouse models if ART1 expression impacts tumor progression and dissemination and the anti-tumor immune response, and (3) to characterize the susceptibility of T cell subsets to ART1-mediated NICD. The first objective relied on histological analysis of ART1 expression and immune cell scoring in a NSCLC tissue microarray (n=493) as well as paired analysis of tumor and matched normal lung tissue from patients with NSCLC for ART1 gene expression by qPCR (n=40), ART1 tissue expression and characterization of $P2X7R^+$ CD8 T cell infiltration by immunofluorescence (n=12) and by flow cytometry (n=5). Mice for in vivo studies were randomly assigned to treatment groups. Sample sizes were determined on the basis of pilot studies to achieve 80% statistical power with a 95% confidence interval. Quantifications of tumor burden and immune cell infiltration were performed in a blinded fashion. Numbers of biological replicates and repeats of each experiment are indicated in the figure legends.

Patient sample collection and analysis

Human lung adenocarcinoma samples for immunofluorescence and flow cytometry staining, as well as RNA extraction and qPCR analysis, were obtained from New York Presbyterian Hospital/Weill Cornell Medical College in accordance with a protocol approved by the IRB (IRB#1008011221). Immunohistochemistry staining for ART1 was performed on a tissue microarray of 493 stage I lung adenocarcinomas (25) (Primary anti-human ART1 antibody: Santa Cruz, Catalog#sc-20255). The tissue microarray was scored in a blinded fashion for intensity and location of ART1 staining. Intensity of ART staining was scored as (1) negative, (2) weak, (3) moderate or (4) strong. Location of staining was scored as (1) cytoplasmic, (2) membranous or (3) both cytoplasmic and membranous. In addition, the tissue microarray was scored for (1) low, (2) intermediate or (3) high infiltration of immune cell subsets; Pan T cells, CD4 T cells, CD8 T cells, T_{reg} cells, B cells, and macrophages in tumor and stroma using CD3, CD4, CD8, FoxP3, CD20, CD56, CD68 and CD163, respectively. NK cell infiltration in tumor and stroma was determined as absent or present using the CD56 marker. The scoring cell number cutoffs are described in table S3.

Animals

All animal work was done following a protocol approved by the Institutional Animal Care and Use Committee of New York Presbyterian Hospital/Weill Cornell Medical College (IACUC # 2010–0050, 2015–0028). Wild type C57BL/6 mice (strain: C57BL/6NTac) and athymic nude mice (strain: B6.Cg/NTac-Foxn1nu NE10) were purchased from Taconic

Biosciences. All mice were maintained under pathogen-free conditions in the Weill Cornell Medicine animal facility. All animal studies were done in accordance with Animal Research: Reporting of In Vivo Experiments (ARRIVE) guidelines.

Animal tumor models

For ART1 knockdown in vivo, doxycycline was delivered to mice in drinking water containing sucrose (0.1 mg/mL doxycycline in 50 g/L sucrose) 48 to 72 hours before injection of KP1 ART1^{OE} cells. Control animals received water containing sucrose only. Water was changed every 4 days. For the orthotopic lung tumor model, 0.5×10^5 KP1 ART1^{OE} cells were resuspended in 100μl phosphate-buffered saline (PBS) and injected into the tail vein of immunocompetent C57BL/6 mice (4 to 6 weeks old). For lung tumor burden evaluation at the indicated endpoints, mice were euthanized, and parts of the tumor-bearing lungs were formalin-fixed, paraffin-embedded and sectioned for subsequent H&E stain and blinded enumeration of lung nodules. The remaining parts of the tumor-bearing lungs were weighed and dissociated into a single cell suspension, stained, and analyzed by flow cytometry for characterization of CD8 T cells as elaborated below. For the ectopic flank tumor model, KP1 ART1^{OE}, B16$^{CONTROL(Scr-6)}$, B16$^{ART1KO\ (42-1)}$ or B16$^{ART1KO\ (63-1)}$ cells were subcutaneously injected into the flank of C57BL/6 mice or immunodeficient nude mice (1×10^5 cells in 50μl PBS). After tumors were palpable, tumor diameters were measured with digital calipers and the tumor volume determined by the formula (length × width^2) /2). In our flank tumor model using B16-F10 CRISPR sublines, we observed that some mice died prior to reaching maximum tumor volumes with evidence of metastatic dissemination. Where indicated, tumors were excised, weighed, and processed for immunofluorescence and flow cytometry analysis as elaborated below.

Antibody-mediated depletion of CD4 and CD8 T cells

For CD8 and CD4 T cell depletion, anti-CD8 (clone: 53–6.7, BioXcell # BP0004–1) and anti-CD4 (clone: GK1.5, BioXcell # BP0003–1) antibodies were i.p. injected per mouse according to the following regimen: day −1 and day 3 (500 μg), then every 72 hours until experiment endpoint (250 μg) (40). As a negative control to CD8 and CD4 depletion, mice from other groups received, by i.p. injection, InVivoPlus rat IgG2a isotype control, anti-trinitrophenol (clone 2A3, BioXcell #BP0089) and InVivoPlus rat IgG2b isotype control, anti-keyhole limpet hemocyanin (clone LTF-2, BioXcell # BP0090), respectively.

22C12 treatment of tumor bearing mice

For flank tumors, intra-tumoral injections started when KP1 ART1^{OE} tumors became palpable on day 11 and every 72 hours until day 23 after tumor inoculation. Mice were injected with 5mg/kg ART1 antibody 22C12 for group ‘22C12’ or Mouse IgG1 isotype control (BioXcell, Cat# BP0297) for group ‘Iso Ctrl’. Tumor sizes were measured every 72 hours and mice were euthanized on day 25 after tumor inoculation, when tumors were weighed and processed for flow cytometry staining. For the orthotopic lung tumor models, mice were injected intravenously with 0.5×10^5 KP1 ART1^{OE} cells on day 0. Where indicated, mice were i.p. injected with 25 mg/kg ART1 antibody 22C12 (22C12) (used in in vivo studies reported in Fig. 3A to F, 3I to K, 4A to C, S4B to H, and fig. S5A to F, S8B, S8E to F). The more recently developed fully humanized 22C12 antibody (22C12 (HuLC))

was used to treat mice i.p. (25 mg/kg) in in vivo studies assessing absolute immune cell counts in tumor-bearing lungs (reported in Fig. 3G and H and fig. S4C, D, G, and H). As controls, mice were treated with 25 mg/kg of Mouse IgG1 isotype control (BioXcell, Cat# BP0297) for group 'Iso Ctrl'. i.p. injections started from day 6 and continued every 72 hours until day 18 as indicated.

Cell Lines

The human cell lines H1650, A549, BEAS2B and HEK293 were obtained from American type culture collection (ATCC) and cultured in RPMI-1640 medium supplemented with 10% fetal bovine serum (FBS) and 1% penicillin/streptomycin in a humidified 5% CO_2 incubator at 37°C. The mouse NSCLC cell line KP1 was previously generated from lung tumors of $KRAS^{G12D/+}/p53^{-/-}$ (KP1) mice (26). Mouse LLC1 lung cancer cells and B16-F10 melanoma cells were obtained from ATCC and cultured in Dulbecco's Modified Eagle's Medium (DMEM) supplemented with 10% FBS and 1% penicillin/streptomycin in a humidified 5% CO_2 incubator at 37°C.

Generation of KP1 $ART1^{OE}$ and inducible hairpin stable cell lines

The pLVX-IRES-tdTomato vector is designed to constitutively coexpress the protein of interest and tdTomato from *P*CMV IE when transduced into mammalian cells. Before transduction, the vector was packaged into viral particles in HEK293T cells, using Lenti-XTM HT Packaging System (Catalog# 632160 and 632161, Takara). The presence of tdTomato allows transductants to be visualized by fluorescence microscopy and sorted by flow cytometry. The *Art1* gene was overexpressed using this construct (pLVX-IRES-td-tomato_ART1). Recombinant lentiviruses (LV) were generated from 293T cells (6×10^6 cells/100 mm plate) by transient transfection of 7μg of lentiviral short hairpin constructs (LT3GENIR) and the lentivirus packaging system (Clontech lenti-x single shot). LV particles were harvested 48 hours and 72 hours later, filtered through 0.45 μm filters, and concentrated by adding lenti-x concentrator (clontech). The LV were then incubated for 30 minutes at 4°C and centrifuging at 1,500 g for 45 minutes at 4 °C. LV particles were used to infect subconfluent cell cultures for 6 hours in the presence of 4 μg/mL polybrene (Sigma-Aldrich). Selection of viral infected cells expressing ART1 was done by sorting for tdTomato positive cells.

shRNA- *LT3GENIR* construct was used to knock down *Art1* genes in KP1 $ART1^{OE}$ cells. The custom designed lentiviral construct expressed short hairpins targeting the *Art1* gene and had green fluorescent protein (GFP) expression for selection. LV were generated as described in the previous section. Selection of virally-infected cells expressing the shRNA was done by using 1 mg/mL G418 (Neomycin analogue, Sigma-Aldrich) in the media. To induce silencing, cells were treated cells with 1μg/ml doxycycline, which induced GFP and shRNA expression. *Art1* shRNA construct #1Antisense Guide Sequence (Art1_87 LT3GENIR) is as follows: TTTGATGTATTCACAGTTGTAT. 97mer.construct sequence is a follows:
TGCTGTTGACAGTGAGCGATAGACATCTTTTCTCAAGAAATAGTGAAGCCACAGAT
GTATTTCTTGAGAAAAGATGTCTAGTGCCTACTGCCTCGGA

CRISPR-mediated gene knockout of *Art1* in B16-F10 cells

CRISPR/Cas9 mediated knockout of *Art1* in B16-F10 cells was performed using Sigma-Aldrich custom-made, ready-to-use DNA plasmids on the U6gRNA:CMV-CAS9–2A-tGFP backbone. Two plasmids containing gRNAs targeting regions in exon 3 of the *Art1* gene were used to create the B16-F10 clones $B16^{ART1KO\ (63-1)}$ (sequence 5'−3': CCTGCGCTTTCGGCCAGCG) and $B16^{ART1KO\ (42-1)}$ (sequence 5'−3': CCAACAAAGTATACGCGGA). A negative control plasmid was used to create the B16-F10 clone $B16^{CONTROL\ (Scr-6)}$ (sequence 5'−3': CGCGATAGCGCGAATATATT). Briefly, B16-F10 cells were seeded in 12 well-plates and incubated for 48 hours to reach 80% confluency. Each CRISPR plasmid (0.5 μg DNA) were mixed with 3 μl TransIT-CRISPR reagent (Sigma-Aldrich) in 100 μg l Opti-MEM medium (Gibco) and incubated at room temperature for 30 minutes. The mixture was added to the B16-F10 cells and incubated in a humidified 5% CO_2 incubator at 37°C for 24 hours. Flow cytometry activated cell sorting (FACS) was used to sort transfected GFP-positive single cells into flat-bottom 96 well-plates. Clones were expanded and tested for ART1 surface expression by flow cytometry and immunofluorescence staining (fig. S3A and B).

Proliferation Assay

1.4×10^4 cells were plated in a 6-well plate. Cells were trypsinized and counted using Cellometer cell counting chambers (Nexcelom Bioscience) every day for four days. For experiments where cells were treated with NAD (20 μM, Sigma-Aldrich, Catalog# N8285) ± 22C12 (20 μg/ml), FBS-supplemented media was replenished with NAD ± 22C12 every 24 hours until the experimental endpoint.

Cell immunofluorescence

Adherent cells were plated in poly-D-lysine coated coverslips and were treated with serum-free media for 12 hours before all experiments. Cells were washed with PBS-CM (1mM $MgCl_2$, 0.1mM $CaCl_2$) and were fixed with 3.7% formaldehyde for 5 minutes (to prevent permeabilization) and incubated with blocking solution (5% bovine serum albumin [BSA] in 1xPBS) for 1 hour in a 37 °C air incubator. The cells were then treated with primary antibody ART1 (Purified ART1 antibody, Pocono, rabbit #2) (1:200) or Poly/Mono-ADP Ribose ('MAR/PAR') (CST, Clone: E6F6A Rabbit mAb Catalog#83732) (1:200) dissolved in 1% BSA (in 1xPBS, referred to as 'cell IF antibody buffer') for one hour in a 37 °C air incubator. Cells were washed with PBS-CM and then incubated with anti-rabbit fluorescent secondary antibody 1:500 (Thermo Fisher Scientific, #A10523) dissolved in 'cell IF antibody buffer' for 30 minutes. Cells were washed with PBS-CM and then stained with 1:1000 Hoechst (HOECHST3342, Thermo Fisher Scientific) in PBS-CM for 5 minutes. Post-washing with PBS-CM, the samples fixed w/ 3.7% formaldehyde for 5 minutes. The samples were then washed in PBS and stored in PBS at 4°C in the dark. Cell fluorescence microscopy was performed using a DMIRB inverted microscope (Leica Microsystems), with a cooled charge-coupled device camera (Princeton Instruments). Images were collected with a 40 × 1.25 numerical aperture objective. MetaMorph software (Universal Imaging) was used for image processing and quantification of MFI and background subtraction.

Dissociation of mouse tissue samples

Mice were euthanized and tumor-bearing lungs were perfused by injection of 10 ml cold PBS through the right ventricle. Lungs and subcutaneous tumors were excised and chopped into small pieces using scalpels. Lung and tumor fragments were transferred to GentleMACS C tubes (Miltenyi, Catalog#130-096-334) after which lung dissociation mix (Miltenyi, Catalog#130-095-927) and mouse tumor dissociation mix (Miltenyi, Catalog#130-096-730) respectively was added to the tubes after preparation according to manufacturer's instructions. Lung and tumor fragments were enzymatically and mechanically digested using the gentleMACS Octo Dissociator with heaters (Miltenyi, Catalog#130-095-937) using program 37C_m_LDK_1 and 37C_m_TDK_1 respectively. Tissue homogenates were resuspended in RPMI-1640 (Corning, Catalog#15-040-CV) supplemented with 10% FBS and passed through a 70 μM strainer (Corning, Catalog#431751) to obtain a single cell suspension. Cells were centrifuged and washed once in cold PBS. Cells were centrifuged and resuspended in a working solution of red blood cell (RBC) Lysis Buffer (eBioscience, Catalog#00-4300-54) and incubated for 2 minutes at room temperature. Cells were washed twice in PBS before proceeding with isolation of T cells or flow cytometry staining.

Dissociation of human tissue samples for flow cytometry

Fresh NSCLC tumor and adjacent normal tissue samples from patients were obtained from the OR/Path (Operating room/Pathology) on ice in DMEM + 10% FBS +1% penicillin/streptomycin. Tissue was washed twice with cold DMEM + 10% FBS +1% penicillin/streptomycin and chopped in DMEM supplemented with the following enzyme cocktail for (Collagenase I 50 U/mL (Worthington Biochemical), Collagenase II 20 U/mL (Worthington Biochemical), Collagenase IV 50 U/mL (Worthington Biochemical), Dnase I 50 Kunitz U/mL (Worthington Biochemical), Elastase 0.075U/mL (Worthington Biochemical). Tissue was digested for 30 minutes at 37 °C, filtered and centrifuged at 4 °C to collect pellet, which was resuspended in ACK lysis buffer that was deactivated using ice cold DMEM + 10% FBS +1% penicillin/streptomycin. The cell pellet was resuspended in FACS buffer [0.5% BSA added to AutoMACS Rinsing Solution (Miltenyi Biotec cat# 130-091-222] prior to staining for flow cytometry.

ADP-ribosylation and NICD assay

Lung single cell suspensions were centrifuged and resuspended in MACS buffer (AutoMACS Rinsing solution (Miltenyi, Catalog#130-091-222) supplemented with 0.5% BSA stock solution (Miltenyi, Catalog#130-091-376)). Isolation of T cells was performed by magnetic bead sorting using Pan T Cell Isolation Kit II, mouse (Miltenyi, Catalog# 130-095-130) according to manufacturer's instructions. Cells were added to 48 well plates pre-coated with rART1 (10 μg/ml) for 24 hours at 4°C prior to co-culture. 1×10^6 T cells were resuspended in serum-free RPMI-1640 medium (Corning, Catalog#15–040-CV) containing 100 μM eNAD (Sigma-Aldrich, Catalog#N2630), 5 μg/ml anti-ART2.2 antibody (s+16a, BioLegend, Catalog# 149801), with or without 30 μg/ml anti-CD38 neutralizing antibody (Clone: NIMR-5, Novus Biologicals, Catalog# NBP2–59506) and with or without 20 μg/ml ART1 blocking 22C12 antibody added to wells. Cells were incubated at 37°C

for 2 hours. T cells were removed from plate by gentle pipetting and transferred to staining plates. T cells were stained with phycoerythrin (PE)-conjugated anti-etheno-NAD antibody for 30 minutes at 4°C (Clone: IG4, Santa Cruz, Catalog#sc-52666, 10 μg/ml) followed by washing in FACS-buffer (PBS supplemented with 2mM EDTA and 0.2% BSA) and staining with surface antibodies CD3 Alexa Fluor (AF) 594 (BioLegend, Catalog#100240, 2.5 μg/ml), CD8α Brilliant Violet (BV) 605 (BioLegend, Catalog#100743, 2.5 μg/ml), CD4 allophycocyanin (APC)-Cy7 ((BioLegend, Catalog#100413, 2.5 μg/ml), CD25 AF488 ((BioLegend, Catalog#102018, 2.5 μg/ml), and P2X7R PE-Cy7 ((BioLegend, Catalog#148707, 5 μg/ml) for 20 minutes at 4°C. DAPI (BioLegend, Catalog#422801, 0.1 μg/ml) was added to the cells 10 minutes prior to acquisition on a FACSymphony Analyzer (BD Biosciences). Flow cytometry data was analyzed using FlowJo software (FlowJo LLC, Becton Dickinson).

Flow Cytometry staining of human and mouse samples

Single cell suspensions derived from enzymatically digested tumor tissue and matched normal lung tissue from patients with lung adenocarcinoma were stained with fixable viability dye (eFluor 780) in PBS for 20 minutes at 4°C. Cells were resuspended in FcR blocking solution (Miltenyi, Catalog# 130-092-575) for 5 minutes followed by addition of P2X7R primary antibody (Novus Biologicals, Clone: 7G1D6 Catalog# NBP2–61748) in FACS buffer for 20 minutes at 4°C. Cells were washed in FACS buffer and resuspended in AF488-conjugated Goat anti-mouse IgG secondary antibody (BioLegend, Catalog#405319) for 20 minutes at 4°C. Cells were washed in FACS buffer and incubated with a master mix of fluorophore-conjugated surface marker antibodies: CD3-Viogreen (Miltenyi, Catalog#130-113-704), CD8-peridinin-chlorophyll-protein (PerCP)-Vio700 (Miltenyi, Catalog#103-113-723), and CD38-PE (eBioscience, Catalog#12-0389-42) for 20 minutes at 4°C.

Single cell suspensions from tumor-bearing mouse lungs or subcutaneous flank tumors were stained with fixable viability dye (eFluor 780) in PBS for 20 min at 4°C. For initial studies cells were washed in FACS buffer and resuspended in a master mix of fluorophore-conjugated surface marker antibodies: CD45-BD Horizon V500 (BD Biosciences, Catalog#561487), CD3-eFluor 450 (eBioscience, Catalog#48-0031-82), CD8β-PE-Vio770 (Miltenyi, Catalog#130-106-316), P2X7R-fluorescein isothiocyanate (FITC, Miltenyi, Catalog#130-114-221). For further studies to characterize CD8 T cell proliferation and activation, master mixes of following conjugated antibodies: CD45-VioBlue (Miltenyi, Catalog# 130-110-802), CD3-FITC (Miltenyi, Catalog# 130-119-798), CD8β-PerCP-Vio700 (Miltenyi, Catalog# 130-111-715), P2X7R-APC (Miltenyi, Catalog# 130-114-330), CD279 (PD-1)-PE (Miltenyi, Catalog# 130-111-953). Cells were permeabilized for staining with Ki67 PE-Vio770 (Miltenyi, Catalog# 130-120-419). To characterize memory T cell populations CD8 T cells the dispersed cells were surface stained in master mixes of following conjugated antibodies: CD69-PE (Miltenyi, Catalog# 130-115-575), CD3-FITC (Miltenyi, Catalog# 130-119-798), CD8β-PerCPVio700 (Miltenyi, Catalog# 130-111-715), P2X7R-APC (Miltenyi, Catalog# 130-114-330), CD62L-VioBlue (Miltenyi, Catalog# 130-112-841) and CD44-PE-Vio770 (Miltenyi, Catalog# 130-110-085). Memory CD8 T cell subsets were classified as follows: T_{CM}, $CD62L^{+}CD44^{+}CD69^{-}$; T_{EM},

$CD62L^{-}CD44^{+}CD69^{-}$; T_{RM}, $CD62L^{-}CD44^{+}CD69^{+}$. Following surface staining, human and mouse cells were washed in FACS buffer and fixed using intracellular (IC) fixation buffer (Invitrogen) for 30 minutes at 4°C. To get absolute counts of immune populations, 30 μl counting beads (CountBright Absolute Counting Beads, 0.52×10^{5} beads/50 μl, Invitrogen # C36950) were added before data acquisition per sample. Absolute counts were calculated using the formula; ((cell event count ×counting bead volume) / (counting bead event count ×cell volume)) × counting bead concentration. Stained samples were acquired on a MACSQuant analyzer and flow cytometry data was analyzed using the FlowJo software (FlowJo LLC, Becton Dickinson).

Frozen Tissue Immunofluorescence

Mouse and patient samples were fixed in formaldehyde and kept in 30% sucrose in PBS until the samples sank. Samples were embedded in optimal cutting temperature (OCT) blocks and sectioned using a cryostat (Leica). Sections were placed on charged slides, demarcated with a barrier pen, and dehydrated in acetone. Sections were then blocked for 1 hour in blocking solution (0.25% Triton-x100+ 5% FBS in 1X PBS). The samples were subjected to overnight incubation in the dark at 4°C with primary purified antibodies. ART1 antibody (Purified ART1 antibody, Pocono, rabbit #2, 1:100), dissolved in antibody buffer (5% FBS dissolved in 1X PBS) was used for ART1 staining of mouse and human patient samples. For CD8 and P2X7R staining of human samples the following antibodies were used: CD8 antibody (YTS105.18) (cat # NB200–578 Novus Biologicals, 1:100) and P2X7/P2RX7 antibody (7G1D6) (NBP2–61748 Novus Biologicals, 1:100). Multiple sections of matched tumor and normal lungs were stained. The samples were washed multiple times in blocking solution and incubated in respective secondary antibodies [1:200 each secondary antibody: Goat anti-Rabbit IgG (H+L) Cross-Adsorbed Secondary antibody conjugated to Cyanine5, cat # A-10523, Thermo Fisher Scientific (secondary to ART1); Goat anti-Rat IgG (H+L) Cross-Adsorbed Secondary antibody conjugated to Alexa Fluor 568, cat # A-11077, Thermo Fisher Scientific (secondary to CD8); Goat anti-Mouse IgG (H+L) Cross-Adsorbed Secondary antibody conjugated to Alexa Fluor 488, cat # A-11001, Thermo Fisher Scientific, (secondary to P2X7/P2RX7)] dissolved in antibody buffer for 1 hour in the dark. The samples were washed multiple times in blocking solution and incubated for 5 minutes with Hoechst (HOECHST3342, Thermo Fisher Scientific, 1:1000 in 1X PBS). Sections were mounted using prolong gold mounting media (# P36934, Thermo Fisher Scientific). Sections were cured overnight at 20°C in dark. Secondary only antibody-stained sections were used to determine specificity of each primary antibody. Fluorescence microscopy was performed using a Zeiss LSM 880 Laser Scanning Confocal Microscope. Multiple fields were acquired from multiple sections of each sample. ImageJ (NIH) was used for image processing, background subtraction, MFI quantification, and cell counting.

Western blot analyses

Cells were treated with serum free media overnight before all experiments. Cells were then treated with NAD^{+} (Sigma-Aldrich, Catalog# N8285) using dose dependent serial dilution (range of 0 to 50 μM) with or without ART1 blocking antibody (20ug/ml 22C12). Cells were washed with PBS and lysed in a mixture of 1X lysis buffer (cat#9803, CST) and Halt Protease & Phosphatase Inhibitor Single-Use Cocktail (cat# 78442, Thermo

Fisher Scientific). Cells were harvested by scraping and centrifuged to collect supernatant. For immunoblot analyses cellular proteins were resolved in 10% SDS-PAGE, transferred to nitrocellulose membranes, and probed with rabbit MAR/PAR antibody (CST #83732, 1:1000). Blots were acquired using MyECL Imager (Thermo Fisher Scientific). Pageruler plus prestained protein ladder, (10 to 250 kDa, # 26619, Thermo Fisher Scientific) was used to determine weights of protein bands.

Quantitative RT-PCR analysis:

Total RNA from cells was extracted with RNA Extraction (QIAGEN RNeasy Mini Kit). For initial studies with tumor cell lines, 500 ng extracted RNA from each well was reversely transcribed to cDNA using the RNA to cDNA EcoDry Premix (Random Hexamers) (catalogue # 639546, Takara). Quantitative PCR was carried out using SYBR green master mix (iQ SYBR Green Supermix, #1708884). The primer sequences for the human and mouse genes are listed in table S4. A C1000 Thermal Cycler (Bio-Rad) was used to perform RT-qPCR, and relative quantification performed using Bio-Rad CFX Manager software. For studies to compare *Art1*, *P2RX7-a* and *P2RX7-k* transcript abundance between lung derived T cells, KP1 lung derived CD8, KP1 lung derived CD4, and tumor lines (KP1, LLC1 and B16), the TaqMan one step qPCR method was utilized. Primers were designed with the aid of Bioinformatics support from Thermo Fisher Scientific. 50 ng RNA was plated into each well and FAM (Fluorescein amidites)-conjugated mouse primers for ‘gene of interest’ *P2X7R-a* (Thermo Fisher Scientific Assay ID: APXGWX4, targeting exon 1, custom made), *P2X7R-k* (Thermo Fisher Scientific Assay ID: APAAF6U, targeting exon 1, custom made), or *Art1* (Thermo Fisher Scientific Assay ID: Mm01274189_m1, targeting exon 4 – 5, amplicon length: 113), as well as VIC (2’-chloro-7’-phenyl-1,4-dichloro-6-carboxyfluorescein)-conjugated *GAPDH* primers as a housekeeping gene (Thermo Fisher Scientific Assay ID: Mm05724508_g1, targeting exon 4), were added to the reaction mix (iTaq Universal Probes One-Step Kit, Bio-Rad # 1725141). Relative mRNA expression was calculated using the $2^{-\Delta\Delta ct}$ method and normalized to relevant house-keeping gene (*GAPDH*).

RNA sequencing and gene expression analysis

CD8 T cells were isolated from untreated mice bearing KP1 lung tumors and RNA sequencing was performed as previously described (41). In order to display gene expression of select genes over the various treatment groups and cell types, Fragments Per Kilobase of transcript per Million mapped reads (FPKM) for each treatment or cell type was imported into R (version 3.6.2). The function ‘pheatmap’ was used to display gene expression as a heatmap and gene expression values were centered and scaled along rows by determining z-score for each value. Clustering was carried out using hierarchical clustering.

TCGA data analysis

cBioPortal was used to visualize and analyze transcriptomic data from the TCGA PanCancer Atlas, lung adenocarcinoma cohort (www.cbioportal.org) (42, 43). Gene expression data of 503 lung adenocarcinoma samples were analyzed. Samples were stratified into mRNA expression data (Batch normalized from Illumina HiSeq_RNASeqV2) using a z score threshold of ±1.0.

NAD-glo assay

A NAD/NADH-Glo Assay (#G9071, Promega) kit was used. Histone (1.5mg/mL), NAD (200nM) (both from the kit) and rART1 (40nM) or denatured ART1 (40nM) enzymes (enzymes were cloned, expressed, and purified by our collaborators at the Tri-Institutional Therapeutic Discovery Institute (TDI)) were added in a 96-well white opaque bottom plate. All the components were added to 1X PBS with a final reaction volume of 50μL per well and incubated on a shaker at 37 °C for 1 hour and equilibrated to room temperature for 5 minutes. The NAD/NADH-Glo Detection Reagent was prepared by mixing 1 mL reconstituted luciferin detection reagent, 5 μL reductase, 5 μL reductase substrate, 5 μL NAD cycling enzyme, and 5 μL NAD cycling substrate by gently inverting 5 times. 50 μL per well of supernatant and 50 μL per well of Detection Reagent was transferred to a new 96-well white luminometer plate, then incubated on a shaker in the dark at room temperature for 30 minutes. The luminescence of the samples was read on a luminometer.

22C12 antibody development and characterization

We collaborated with the Biologics group at the Tri-Institutional Therapeutic Discovery Institute (TDI) to develop monoclonal ART1 binding and blocking antibodies, utilizing the AlivaMab Mouse (Ablexis, LLC) transgenic mouse strains comprising of human immunoglobulin repertoires. To generate functional human antibodies against ART1, purified recombinant human and mouse ART1 produced in HEK293 mammalian cells was used to immunize AlivaMab mouse strains, both AlivaMab Mouse Kappa and AlivaMab Mouse Lambda. The first-generation version of the latter also expressed mouse kappa immunoglobulin light chains. Following generation of hybridomas from splenocytes, hybridomas expressing antibodies with the desired characteristics were identified utilizing a rigorous screening funnel developed by the TDI. First, hybridoma supernatants were screened by enzyme-linked immunosorbent assay (ELISA) using plates coated with purified human ART1. Anti-human ART1 positive hybridoma supernatants were then tested for inhibition of purified human ART1 by a fluorescent NAD^+ readout (Abcam, cat. ab176723). Anti-ART1 hybridoma supernatants were also tested for inhibition of human ART1 transiently expressed in HEK293 cells using the eNAD-based ADP-ribosylation assay (30). The hybridoma supernatants clone 22C12, derived from immunization of AlivaMab Mouse Lambda, was positive for inhibition of human ART1 in the biochemical and cell-based assays. Supernatants from 22C12 were then tested for binding to murine ART1 by ELISA and enzymatic inhibition of purified mouse ART1.

We next tested binding affinity of 22C12 to human and mouse ART1. Following hybridoma subcloning and expansion of clone 22C12, the antibody was purified from hybridoma supernatant for potency ranking and affinity determination by bioluminescence (BLI). A range of concentrations of purified mouse and human light chain 22C12 antibodies and purified human or mouse ART1 was used to determine the dissociation constant (K_D).

Dose-dependent inhibition of surface ADP-ribosylation by 22C12 was tested. To determine potency in the cell-based functional assay, purified 22C12 antibody was incubated with HEK293 cells transiently transfected with human ART1 at different concentrations prior

to treatment with eNAD. Cell-surface ADP-ribosylation was then determined by flow cytometry and used to calculate IC_{50} values.

Statistical analysis

For the NSCLC tissue microarray, continuous variables are reported as median (interquartile range [IQR]) and categorical variables are reported as count (percent). Chi-square or Fisher's exact tests were used to compare a categorical variable between independent groups. A Mann-Whitney U test was used to compare a continuous variable between two independent groups. Wilcoxon signed rank test was used to assess statistically significant differences in gene expression data from paired samples. A paired t-test was used to determine statistically significant differences in *ART1* expression determined by immunofluorescence surface staining in paired samples. *ART1* expression data were square root transformed, and percentages of tissue-infiltrating immune cells were log-transformed prior to statistical testing by paired t-test to ensure the underlying assumptions of the test were met. Statistically significant differences in ART1 MFI on human lung tumor cell lines was determined by one-way analysis of variance (ANOVA) with Tukey's test for multiple comparisons.

For mouse experiments, data consisting of counts, percentages and expression data were log-transformed or square root transformed where indicated prior to statistical testing by Welch's t-test. Tumor growth data comparing the effect of induced *Art1*-knockdown in KP1 ART1^{OE} tumors or *Art1* knockout in B16-F10 tumors were analyzed by repeated-measures ANOVA with Geisser-Greenhouse correction. A mixed model analysis was used to determine statistically significant difference in flank tumor growth between mice treated with ART1-blocking antibody or isotype control antibody. Statistically significant differences in lung tumor burden between groups of mice treated with or without ART1 blockade in the setting of CD8 and CD4 depletion, differences in ADP-ribosylation and NICD between treatment in eNAD assays, as well as differences in ART1 MFI on KP1 cells and KP1 ART1^{OE} with or without shART1 induction was determined by one-way ANOVA with Tukey's test for multiple comparisons. All statistical tests were two-sided and considered statistically significant with $p < 0.05$. Data analysis was performed using SPSS software version 25 (IBM Corp.) or GraphPad Prism Version 8 (GraphPad).

Supplementary Material

Refer to Web version on PubMed Central for supplementary material.

Acknowledgements

We acknowledge the Electron Microscopy & Histology Core of Weill Cornell Medicine for assistance in tissue processing and H&E staining. We thank Sharrell B. Lee, Najla Saadallah, Pramodh Seneviratne, Arshdeep Singh and Shashi Kariyawasam for technical assistance.

Funding

This work was supported by a Department of Defense Lung Cancer Research Program Grant (W81XWH-19-1-0422) and a Lung Cancer Research Foundation Grant (5327232803) to BS and TEM; BS receives research support from the American Association for Thoracic Surgery and the Graham Foundation. Support was

provided by the National Institutes of Health grant R01CA198533 (to SD). EW receives research support from The Institute of Cancer Research / Royal Marsden (ICR/RM) Cancer Research UK RadNet Centre.

Competing Interests

BS is a consultant for Pfizer, AstraZeneca, and Flame Biosciences. BS is on the advisory board or a speaker for Pfizer, AstraZeneca, BMS, and Genentech (Board: Lung Cancer Research Foundation, AATS Foundation Council). BS discloses holding stock or salary in Pfizer, PPD (Pharmaceutical Product Development). BS was paid a speaker fee by Ribon Therapeutics for work related to this topic. BS is a consultant at Flame Biosciences and Galvanize Therapeutics. BS's wife is an employee and has financial interest in Xalud Therapeutics. TM has received a research grant from Pfizer for an unrelated project. SD has received compensation for consultant/advisory services from Lytix Biopharma, Mersana Therapeutics, EMD Serono, Ono Pharmaceutical, and Genentech, and research support from Lytix Biopharma and Boehringer-Ingelheim for unrelated projects. TW's Equity holdings include unvested RSU's, AstraZeneca. ICL is a paid consultant for Ceramedix Holding, Kairos Ventures, Kiniksa Pharmaceuticals, Rgenix, and X-Vax Technology. BS, TM, IL, and TW are inventors on patent/patent application (1676.171PRV(2088141×7ADA8)) held/submitted by Weill Cornell Medical College that covers the material antibody and its derivatives, as well as a method to prevent, inhibit, or treat ART1-mediated immunosuppression in mammals.. EW, SM, CH, CA, CC, AVM, SS, NR, SVN, MKK, AN, NN, VM, GM, XKZ, PA, AB, TEW, AGK, and NA have declared no conflicts of interest.

Data and materials availability

All data associated with this study are available in the main text or the supplementary materials. ART1 overexpressing, knockdown, and knockout cell lines (KP1 ART1^{OE}, KP1 ART1^{OE} shART1, B16^{ART1KO}) are available from Timothy McGraw under a material transfer agreement with Cornell University.

References and Notes:

1. Mok TSK, Wu YL, Kudaba I, Kowalski DM, Cho BC, Turna HZ, Castro G Jr., Srimuninnimit V, Laktionov KK, Bondarenko I, Kubota K, Lubiniecki GM, Zhang J, Kush D, Lopes G, K.−. Investigators, Pembrolizumab versus chemotherapy for previously untreated, PD-L1-expressing, locally advanced or metastatic non-small-cell lung cancer (KEYNOTE-042): a randomised, open-label, controlled, phase 3 trial. Lancet 393, 1819–1830 (2019). [PubMed: 30955977]
2. Reck M, Rodriguez-Abreu D, Robinson AG, Hui R, Csoszi T, Fulop A, Gottfried M, Peled N, Tafreshi A, Cuffe S, O'Brien M, Rao S, Hotta K, Leiby MA, Lubiniecki GM, Shentu Y, Rangwala R, Brahmer JR, K.−. Investigators, Pembrolizumab versus Chemotherapy for PD-L1-Positive Non-Small-Cell Lung Cancer. N Engl J Med 375, 1823–1833 (2016). [PubMed: 27718847]
3. Gandhi L, Rodriguez-Abreu D, Gadgeel S, Esteban E, Felip E, De Angelis F, Domine M, Clingan P, Hochmair MJ, Powell SF, Cheng SY, Bischoff HG, Peled N, Grossi F, Jennens RR, Reck M, Hui R, Garon EB, Boyer M, Rubio-Viqueira B, Novello S, Kurata T, Gray JE, Vida J, Wei Z, Yang J, Raftopoulos H, Pietanza MC, Garassino MC, K.−. Investigators, Pembrolizumab plus Chemotherapy in Metastatic Non-Small-Cell Lung Cancer. N Engl J Med 378, 2078–2092 (2018). [PubMed: 29658856]
4. Gandini S, Massi D, Mandala M, PD-L1 expression in cancer patients receiving anti PD-1/PD-L1 antibodies: A systematic review and meta-analysis. Crit Rev Oncol Hematol 100, 88–98 (2016). [PubMed: 26895815]
5. Balducci E, Horiba K, Usuki J, Park M, Ferrans VJ, Moss J, Selective expression of RT6 superfamily in human bronchial epithelial cells. Am J Respir Cell Mol Biol 21, 337–346 (1999). [PubMed: 10460751]
6. Stevens LA, Levine RL, Gochuico BR, Moss J, ADP-ribosylation of human defensin HNP-1 results in the replacement of the modified arginine with the noncoded amino acid ornithine. Proc Natl Acad Sci U S A 106, 19796–19800 (2009). [PubMed: 19897717]
7. Okazaki IJ, Zolkiewska A, Nightingale MS, Moss J, Immunological and structural conservation of mammalian skeletal muscle glycosylphosphatidylinositol-linked ADP-ribosyltransferases. Biochemistry 33, 12828–12836 (1994). [PubMed: 7947688]

8. Tang Y, Wang YL, Yang L, Xu JX, Xiong W, Xiao M, Li M, Inhibition of arginine ADP-ribosyltransferase 1 reduces the expression of poly(ADP-ribose) polymerase-1 in colon carcinoma. Int J Mol Med 32, 130–136 (2013). [PubMed: 23652727]
9. Yang L, Xiao M, Li X, Tang Y, Wang YL, Arginine ADP-ribosyltransferase 1 promotes angiogenesis in colorectal cancer via the PI3K/Akt pathway. Int J Mol Med 37, 734–742 (2016). [PubMed: 26847718]
10. Song GL, Jin CC, Zhao W, Tang Y, Wang YL, Li M, Xiao M, Li X, Li QS, Lin X, Chen WW, Kuang J, Regulation of the RhoA/ROCK/AKT/beta-catenin pathway by arginine-specific ADP-ribosytransferases 1 promotes migration and epithelial-mesenchymal transition in colon carcinoma. Int J Oncol 49, 646–656 (2016). [PubMed: 27277835]
11. Burnstock G, Knight GE, Cellular distribution and functions of P2 receptor subtypes in different systems. Int Rev Cytol 240, 31–304 (2004). [PubMed: 15548415]
12. Adinolfi E, Capece M, Franceschini A, Falzoni S, Giuliani AL, Rotondo A, Sarti AC, Bonora M, Syberg S, Corigliano D, Pinton P, Jorgensen NR, Abelli L, Emionite L, Raffaghello L, Pistoia V, Di Virgilio F, Accelerated tumor progression in mice lacking the ATP receptor P2X7. Cancer Res 75, 635–644 (2015). [PubMed: 25542861]
13. Haag F, Adriouch S, Brass A, Jung C, Moller S, Scheuplein F, Bannas P, Seman M, Koch-Nolte F, Extracellular NAD and ATP: Partners in immune cell modulation. Purinergic Signal 3, 71–81 (2007). [PubMed: 18404420]
14. Di Virgilio F, Sarti AC, Falzoni S, De Marchi E, Adinolfi E, Extracellular ATP and P2 purinergic signalling in the tumour microenvironment. Nat Rev Cancer 18, 601–618 (2018). [PubMed: 30006588]
15. Boldrini L, Giordano M, Ali G, Melfi F, Romano G, Lucchi M, Fontanini G, P2X7 mRNA expression in non-small cell lung cancer: MicroRNA regulation and prognostic value. Oncol Lett 9, 449–453 (2015). [PubMed: 25436007]
16. Scheuplein F, Schwarz N, Adriouch S, Krebs C, Bannas P, Rissiek B, Seman M, Haag F, Koch-Nolte F, NAD+ and ATP released from injured cells induce P2X7-dependent shedding of CD62L and externalization of phosphatidylserine by murine T cells. J Immunol 182, 2898–2908 (2009). [PubMed: 19234185]
17. Sandoval-Montes C, Santos-Argumedo L, CD38 is expressed selectively during the activation of a subset of mature T cells with reduced proliferation but improved potential to produce cytokines. Journal of leukocyte biology 77, 513–521 (2005). [PubMed: 15618297]
18. Chen L, Diao L, Yang Y, Yi X, Rodriguez BL, Li Y, Villalobos PA, Cascone T, Liu X, Tan L, Lorenzi PL, Huang A, Zhao Q, Peng D, Fradette JJ, Peng DH, Ungewiss C, Roybal J, Tong P, Oba J, Skoulidis F, Peng W, Carter BW, Gay CM, Fan Y, Class CA, Zhu J, Rodriguez-Canales J, Kawakami M, Byers LA, Woodman SE, Papadimitrakopoulou VA, Dmitrovsky E, Wang J, Ullrich SE, Wistuba II, Heymach JV, Qin FX, Gibbons DL, CD38-Mediated Immunosuppression as a Mechanism of Tumor Cell Escape from PD-1/PD-L1 Blockade. Cancer Discov 8, 1156–1175 (2018). [PubMed: 30012853]
19. Adriouch S, Hubert S, Pechberty S, Koch-Nolte F, Haag F, Seman M, NAD+ released during inflammation participates in T cell homeostasis by inducing ART2-mediated death of naive T cells in vivo. J Immunol 179, 186–194 (2007). [PubMed: 17579037]
20. Stark R, Wesselink TH, Behr FM, Kragten NAM, Arens R, Koch-Nolte F, van Gisbergen K, van Lier RAW, T RM maintenance is regulated by tissue damage via P2RX7. Sci Immunol 3, (2018).
21. Nizard M, Roussel H, Diniz MO, Karaki S, Tran T, Voron T, Dransart E, Sandoval F, Riquet M, Rance B, Marcheteau E, Fabre E, Mandavit M, Terme M, Blanc C, Escudie JB, Gibault L, Barthes FLP, Granier C, Ferreira LCS, Badoual C, Johannes L, Tartour E, Induction of resident memory T cells enhances the efficacy of cancer vaccine. Nat Commun 8, 15221 (2017). [PubMed: 28537262]
22. Hubert S, Rissiek B, Klages K, Huehn J, Sparwasser T, Haag F, Koch-Nolte F, Boyer O, Seman M, Adriouch S, Extracellular NAD+ shapes the Foxp3+ regulatory T cell compartment through the ART2-P2X7 pathway. J Exp Med 207, 2561–2568 (2010). [PubMed: 20975043]
23. Haag F, Koch-Nolte F, Kuhl M, Lorenzen S, Thiele HG, Premature stop codons inactivate the RT6 genes of the human and chimpanzee species. J Mol Biol 243, 537–546 (1994). [PubMed: 7966280]

24. Du X, Low MG, Down-regulation of glycosylphosphatidylinositol-specific phospholipase D induced by lipopolysaccharide and oxidative stress in the murine monocyte- macrophage cell line RAW 264.7. Infect Immun 69, 3214–3223 (2001). [PubMed: 11292743]
25. Suzuki K, Kadota K, Sima CS, Nitadori J, Rusch VW, Travis WD, Sadelain M, Adusumilli PS, Clinical impact of immune microenvironment in stage I lung adenocarcinoma: tumor interleukin-12 receptor beta2 (IL-12Rbeta2), IL-7R, and stromal FoxP3/CD3 ratio are independent predictors of recurrence. J Clin Oncol 31, 490–498 (2013). [PubMed: 23269987]
26. Choi H, Sheng J, Gao D, Li F, Durrans A, Ryu S, Lee SB, Narula N, Rafii S, Elemento O, Altorki NK, Wong ST, Mittal V, Transcriptome analysis of individual stromal cell populations identifies stroma-tumor crosstalk in mouse lung cancer model. Cell Rep 10, 1187–1201 (2015). [PubMed: 25704820]
27. Simon S, Labarriere N, PD-1 expression on tumor-specific T cells: Friend or foe for immunotherapy? Oncoimmunology 7, e1364828 (2017). [PubMed: 29296515]
28. Borges da Silva H, Beura LK, Wang H, Hanse EA, Gore R, Scott MC, Walsh DA, Block KE, Fonseca R, Yan Y, Hippen KL, Blazar BR, Masopust D, Kelekar A, Vulchanova L, Hogquist KA, Jameson SC, The purinergic receptor P2RX7 directs metabolic fitness of long-lived memory CD8(+) T cells. Nature 559, 264–268 (2018). [PubMed: 29973721]
29. Borges da Silva H, Peng C, Wang H, Wanhainen KM, Ma C, Lopez S, Khoruts A, Zhang N, Jameson SC, Sensing of ATP via the Purinergic Receptor P2RX7 Promotes CD8(+) Trm Cell Generation by Enhancing Their Sensitivity to the Cytokine TGF-beta. Immunity 53, 158–171 e156 (2020). [PubMed: 32640257]
30. Krebs C, Koestner W, Nissen M, Welge V, Parusel I, Malavasi F, Leiter EH, Santella RM, Haag F, Koch-Nolte F, Flow cytometric and immunoblot assays for cell surface ADP-ribosylation using a monoclonal antibody specific for ethenoadenosine. Anal Biochem 314, 108–115 (2003). [PubMed: 12633608]
31. Koch-Nolte F, Reyelt J, Schossow B, Schwarz N, Scheuplein F, Rothenburg S, Haag F, Alzogaray V, Cauerhff A, Goldbaum FA, Single domain antibodies from llama effectively and specifically block T cell ecto-ADP-ribosyltransferase ART2.2 in vivo. FASEB J 21, 3490–3498 (2007). [PubMed: 17575259]
32. Schwarz N, Drouot L, Nicke A, Fliegert R, Boyer O, Guse AH, Haag F, Adriouch S, Koch-Nolte F, Alternative splicing of the N-terminal cytosolic and transmembrane domains of P2X7 controls gating of the ion channel by ADP-ribosylation. PLoS One 7, e41269 (2012). [PubMed: 22848454]
33. Sharma P, Allison JP, The future of immune checkpoint therapy. Science 348, 56–61 (2015). [PubMed: 25838373]
34. Taube JM, Galon J, Sholl LM, Rodig SJ, Cottrell TR, Giraldo NA, Baras AS, Patel SS, Anders RA, Rimm DL, Cimino-Mathews A, Implications of the tumor immune microenvironment for staging and therapeutics. Mod Pathol 31, 214–234 (2018). [PubMed: 29192647]
35. Xu JX, Xiong W, Zeng Z, Tang Y, Wang YL, Xiao M, Li M, Li QS, Song GL, Kuang J, Effect of ART1 on the proliferation and migration of mouse colon carcinoma CT26 cells in vivo. Mol Med Rep 15, 1222–1228 (2017). [PubMed: 28138708]
36. De Marchi E, Orioli E, Pegoraro A, Sangaletti S, Portararo P, Curti A, Colombo MP, Di Virgilio F, Adinolfi E, The P2X7 receptor modulates immune cells infiltration, ectonucleotidases expression and extracellular ATP levels in the tumor microenvironment. Oncogene 38, 3636–3650 (2019). [PubMed: 30655604]
37. Ghiringhelli F, Apetoh L, Tesniere A, Aymeric L, Ma Y, Ortiz C, Vermaelen K, Panaretakis T, Mignot G, Ullrich E, Perfettini JL, Schlemmer F, Tasdemir E, Uhl M, Genin P, Civas A, Ryffel B, Kanellopoulos J, Tschopp J, Andre F, Lidereau R, McLaughlin NM, Haynes NM, Smyth MJ, Kroemer G, Zitvogel L, Activation of the NLRP3 inflammasome in dendritic cells induces IL-1beta-dependent adaptive immunity against tumors. Nat Med 15, 1170–1178 (2009). [PubMed: 19767732]
38. Quezada SA, Peggs KS, Curran MA, Allison JP, CTLA4 blockade and GM-CSF combination immunotherapy alters the intratumor balance of effector and regulatory T cells. J Clin Invest 116, 1935–1945 (2006). [PubMed: 16778987]

39. Fabrizio G, Di Paola S, Stilla A, Giannotta M, Ruggiero C, Menzel S, Koch-Nolte F, Sallese M, Di Girolamo M, ARTC1-mediated ADP-ribosylation of GRP78/BiP: a new player in endoplasmic-reticulum stress responses. Cell Mol Life Sci 72, 1209–1225 (2015). [PubMed: 25292337]

40. Zamarin D, Holmgaard RB, Subudhi SK, Park JS, Mansour M, Palese P, Merghoub T, Wolchok JD, Allison JP, Localized oncolytic virotherapy overcomes systemic tumor resistance to immune checkpoint blockade immunotherapy. Sci Transl Med 6, 226ra232 (2014).

41. Markowitz GJ, Havel LS, Crowley MJ, Ban Y, Lee SB, Thalappillil JS, Narula N, Bhinder B, Elemento O, Wong ST, Gao D, Altorki NK, Mittal V, Immune reprogramming via PD-1 inhibition enhances early-stage lung cancer survival. JCI Insight 3, (2018).

42. Cerami E, Gao J, Dogrusoz U, Gross BE, Sumer SO, Aksoy BA, Jacobsen A, Byrne CJ, Heuer ML, Larsson E, Antipin Y, Reva B, Goldberg AP, Sander C, Schultz N, The cBio cancer genomics portal: an open platform for exploring multidimensional cancer genomics data. Cancer Discov 2, 401–404 (2012). [PubMed: 22588877]

43. Gao J, Aksoy BA, Dogrusoz U, Dresdner G, Gross B, Sumer SO, Sun Y, Jacobsen A, Sinha R, Larsson E, Cerami E, Sander C, Schultz N, Integrative analysis of complex cancer genomics and clinical profiles using the cBioPortal. Sci Signal 6, pl1 (2013).

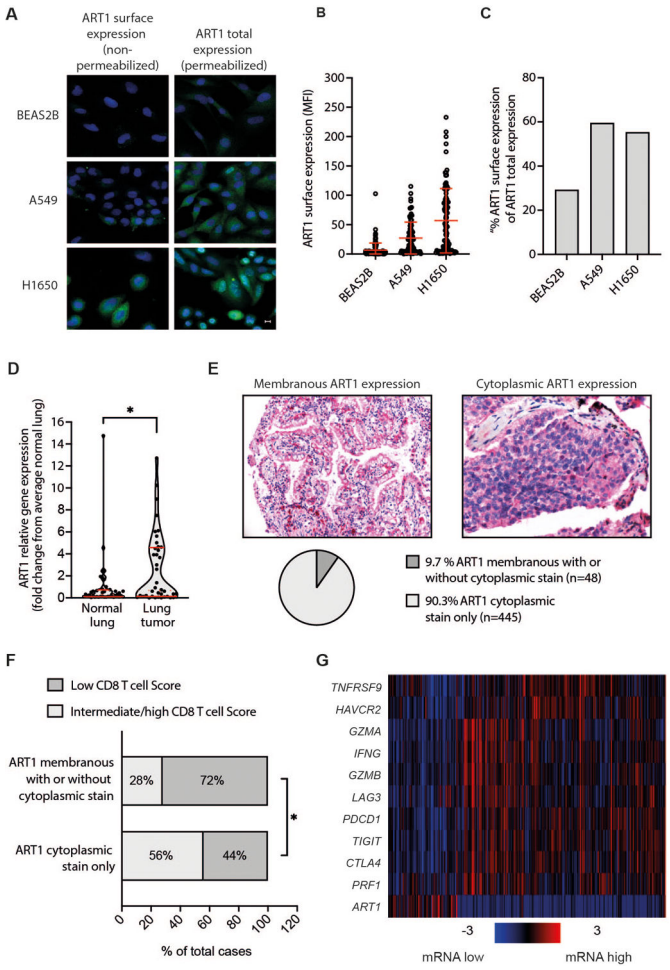

Figure 1. ART1 is overexpressed in a subset of human lung cancers.

(**A and B**) ART1 immunofluorescence staining is shown for human lung cancer cell lines A549 and H1650 and benign bronchial epithelium cell line BEAS2B. (**A**) Representative pictures show ART1 surface expression in non-permeabilized cells (left column) and ART1 total cell expression in permeabilized cells (right column). Scale bar indicates 10 μm. (**B**) Mean fluorescence intensity (MFI) of ART1 surface staining is shown for A549, H1650, and BEAS2B cells (n=1). Each dot represents the ART1 MFI of one cell. Error bars indicate mean with standard deviation (SD) (**C**) The ratio of ART1 surface MFI and ART1 total MFI (as shown in in fig. S1A) in BEAS2B, A549, and H1650 cells (n=1) is shown. (**D**) The violin plot depicts *ART1* qPCR analysis of matched lung tumor tissue and normal lung tissue from patients with stage I to III lung adenocarcinoma (n=40); data were analyzed using a Wilcoxon matched pairs signed rank test. Median is indicated by dotted red line, quartiles are indicated by solid red lines. (**E and F**) ART1 expression was analyzed by immunohistochemistry in a human tissue microarray containing 493 stage I adenocarcinomas. Localization of ART1 expression was scored as (1) membranous (with or without cytoplasmic staining) or (2) tumor cell cytoplasm only. Tumors were scored for infiltration of immune cells (listed in table S3). (**E**) Representative immunohistochemistry images and pie chart show the percentage of tumors that stained positive for ART1

membranous expression or ART1 expression in the cytoplasm only. (**F**) The percentage of tumors with a low or intermediate/high CD8 T cell score is shown for tumors with membranous ART1 staining or cytoplasmic ART1 staining only. Data in (F) were analyzed by a Chi-square test. Gene expression data were square root-transformed prior to statistical testing. *p<0.05. (**G**) mRNA expression of *ART1*, as well as genes associated with CD8 T cell cytotoxicity and immunoregulation, were quantified using data from patients with lung adenocarcinoma from the TCGA PanCancer Atlas cohort (n=503). CD8 T cell cytotoxicity genes analyzed include IFN-γ (*IFNG*), Granzyme A (*GZMA*), Granzyme B (*GZMB*), Perforin 1 (*PRF1*) 41BB (*TNFRSF9*); immunoregulatory genes analyzed include CTLA-4 (*CTLA4*), PD-1 (*PDCD1*), Tim-3 (*HAVCR2*), Lag-3 (*LAG3*) and Tigit (*TIGIT*). The clustered OncoPrint heatmap depicts mRNA expression z-scores relative to all samples.

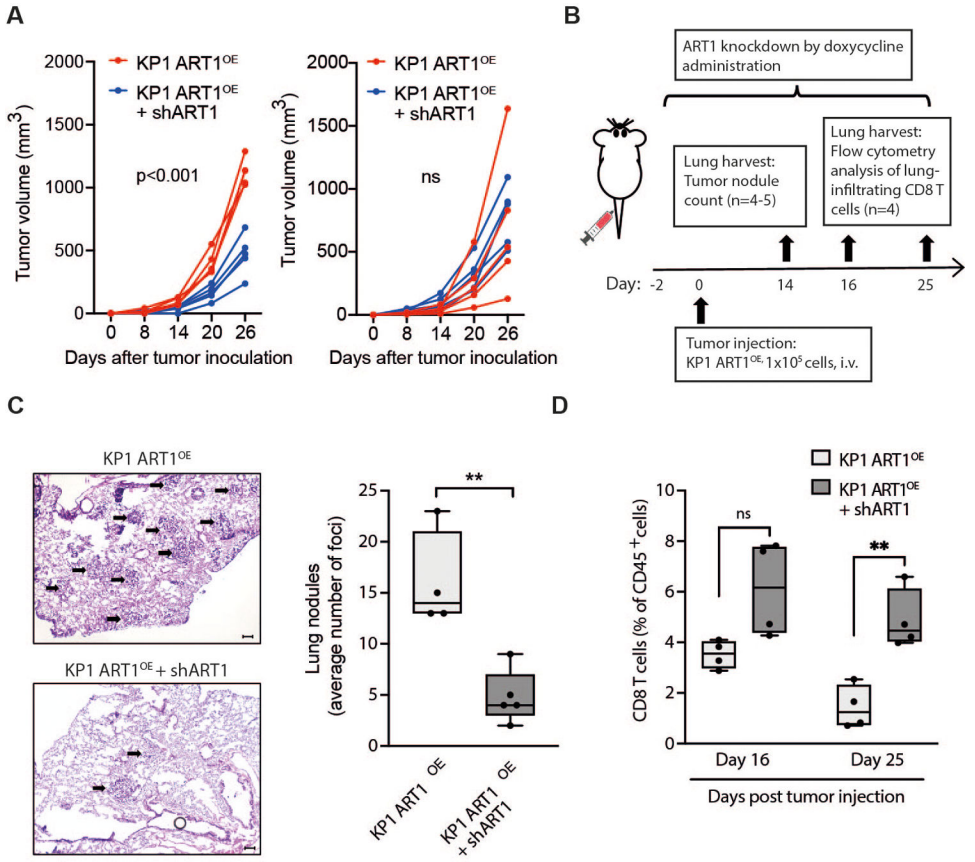

Figure 2. ART1 expression promotes tumor growth in murine lung tumor models.

(**A**) An ectopic subcutaneous (s.c.) flank tumor model was used to assess growth of KP1 ART1^{OE} tumors in wild type and immunodeficient nude mice. KP1 cells were stably transduced with ART1 overexpression lentiviral vector (KP1 ART1^{OE}) and subsequently transduced with shRNA targeting ART1 (shART1). Mice were treated with doxycycline-treated water ad libitum to induce shART1 starting two days before flank tumor inoculation. Growth curves of subcutaneous KP1 ART1^{OE} flank tumors are shown for immunocompetent wild type C57BL/6 mice (left panel, n = 5 mice per group) and for immunodeficient athymic nude mice (right panel, n = 5 mice per group). Statistically significant differences in tumor growth between groups was determined by repeated-measures ANOVA. The experiment was performed twice with similar results. (**B**) An orthotopic KP1 ART1^{OE} lung tumor model administered intravenously (i.v.) was used to assess lung tumor burden and lung infiltration of CD8 T cells. Where indicated, mice were treated with doxycycline-treated water ad libitum to induce shART1. (**C**) Representative images of lung sections stained with H&E (left panels) and enumeration of lung nodules (right panel) are shown for mice euthanized on day 14 after injection of KP1 ART1^{OE} (n = 4 to 5 mice per group). Data in (C) were analyzed using Welch's t-test. Lung nodules in H&E stained images are indicated by black arrows. Scale bar indicates 100 μm. Tumor nodule counts were determined using Image J software. (**D**) Percentage of CD8 T cells among total lung-infiltrating leukocytes (CD45^{+} cells) at day 16 and 25 after tumor injection. Data in (D) were analyzed using Welch's t-test. Experiment was performed three times with similar results. Box plots shows median

and 10^{th} and 90^{th} percentiles; whiskers indicate minimum and maximum values. Percentage and count data were square root-transformed prior to statistical testing. ns, not significant; **p<0.01.

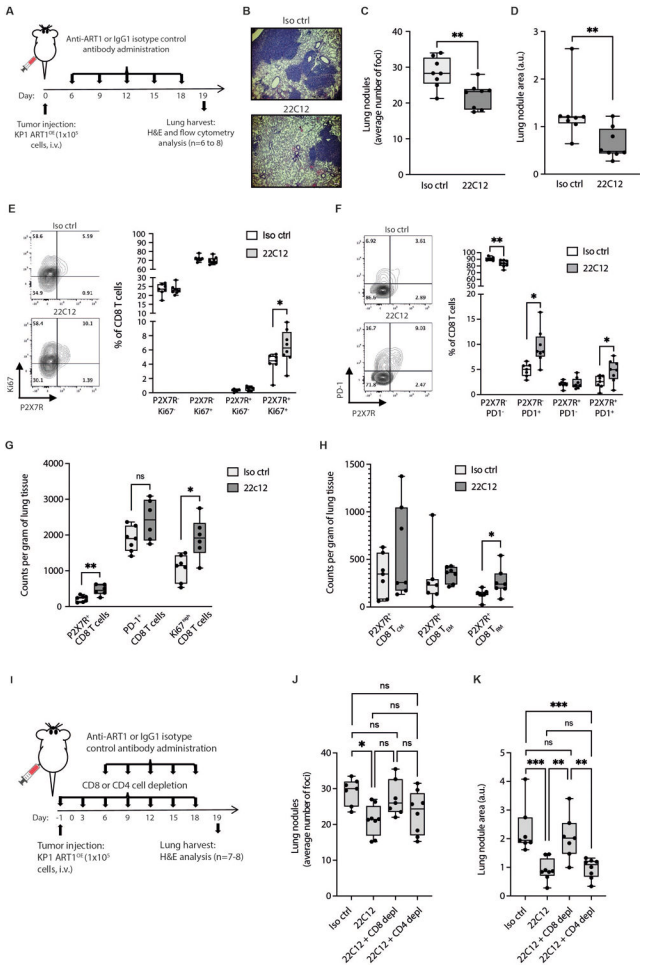

Figure 3. ART1 blockade reduces lung tumor burden and promotes infiltration of P2X7R$^+$ CD8 T cells.

(**A**) An in vivo experiment was used to study lung tumor burden and lung immune cell analysis in mice orthotopically inoculated by i.v. injections with KP1 ART1^{OE} tumors. One group of mice received intraperitoneal (i.p.) treatment with ART1 blocking antibody, 22C12 for (A to F) and 22C12 (HuLC) for (G and H), and the other group received isotype matched control antibody (iso ctrl) every three days starting on day 6 until day 18 (n=7 to 8 mice per group). The experiment was repeated once with similar results. (**B**) Representative H&E staining images of sections of mouse lungs are shown. Scale bar indicates 100 μm. (**C**) Average lung tumor nodule counts and (**D**) average lung nodule area were measured on day 19 after tumor inoculation. Data in (C and D) were analyzed using Welch's t-test. (**E to H**) Immune phenotyping by flow cytometry is shown for digested mouse lungs collected on day 19 following treatment with 22C12 or iso ctrl antibodies. (**E**) Representative dot plots and box plots showing the percentage of CD8 T cells expressing P2X7R with or without the proliferation marker, Ki67. (**F**) Representative dot plots and box plots showing the percentage of CD8 T cells expressing P2X7R with or without the immunoregulatory receptor, PD-1. (**G**) Absolute counts of P2X7R$^+$ CD8 T cells, PD-1$^+$ CD8 T cells, and Ki67^{high} CD8 T cells per gram of tumor-bearing lung tissue are shown for the KP1 ART1^{OE} lung tumor model on day 25 after tumor cell injection (n=6 to 7 per group). (**H**) Absolute

counts of $P2X7R^+$ CD8 T_{CM}, $P2X7R^+$ CD8 T_{EM}, and $P2X7R^+$ CD8 T_{RM} cells per gram of tumor-bearing lung tissue are shown for the KP1 $ART1^{OE}$ lung tumor model on day 25 after tumor cell injection (n=6 to 7 per group). The experiment was performed three times with similar results. Box plots shows median and 10^{th} and 90^{th} percentiles; whiskers indicate minimum and maximum values. Data in (E to H) were analyzed using Welch's t-test. Percentage and count data were square root transformed prior to statistical testing. (**I**) An in vivo experiment was used to study the effect of CD8 T cell and CD4 T cell depletion on the anti-tumor effect of ART1 blockade. Mice were orthotopically inoculated by tail vein injection with KP1 $ART1^{OE}$ tumors on day 0. Where indicated, mice received i.p. treatment with ART1 blocking antibody (22C12) or isotype matched control antibody (iso ctrl) (25 mg/kg), CD8 depleting (depl) antibodies (clone: 53–6.7) or CD4 depleting antibodies (clone: GK1.5) at a dose of 500 μg on day −1 followed by 250 μg every three days from day 3 to 18 (n=7 to 8 mice per group). (**J**) Average lung tumor nodule counts and (**K**) average lung nodule area on day 19 after tumor inoculation are shown. Tumor nodule counts and area were determined using Image J software. a.u. indicates arbitrary units. Box plots shows median and 10^{th} and 90^{th} percentiles; whiskers indicate minimum and maximum values. Data in (J and K) were analyzed using a one-way ANOVA with Tukey's test for multiple comparisons. Percentage and count data were square root-transformed prior to statistical testing. ns, not significant; *p<0.05, **p<0.01, ***p<0.001.

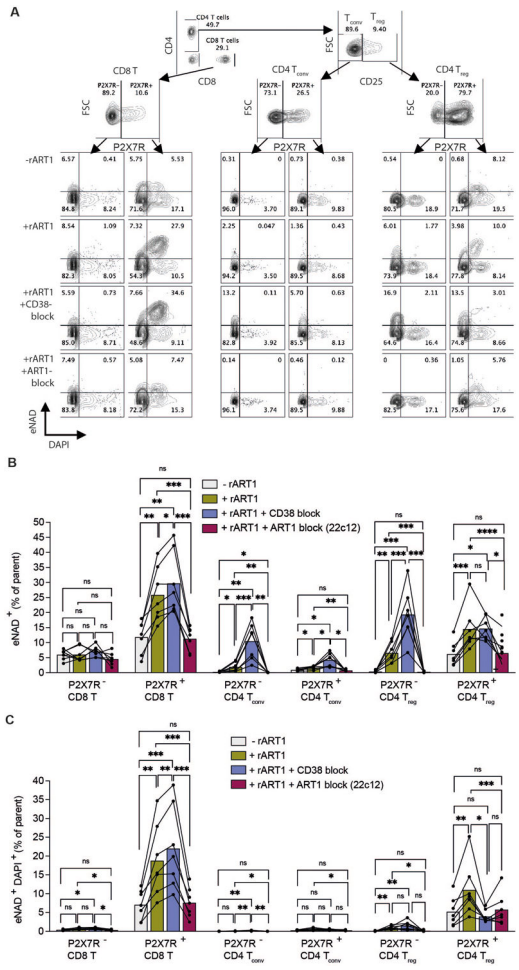

Figure 4. ART1 mediates ADP-ribosylation and NICD of lung tumor-infiltrating T cell subsets.

T cells isolated from wild type KP1 tumor bearing lungs of C57BL/6 mice were incubated for two hours with etheno-NAD (eNAD) alone (-rART1) or with eNAD and rART1, CD38 blocking antibody (NIMR-5) (CD38 block) or ART1 blocking antibody (ART1 block (22C12)). In order to exclusively measure ART1-blockade, ART2 activity was blocked in all culture conditions using an ART2-blocking nanobody (s+16a). After co-culture, T cells were analyzed by flow cytometry for ADP-ribosylation by eNAD staining and for cell death by DAPI staining (n=7). (**A**) An example gating strategy is shown, depicting identification of CD8 T cells (CD8 T), CD4 T_{conv} ($CD4^+CD25^-$) and CD4 T_{reg} ($CD4^+CD25^+$) cells. FSC, forward scatter. The $P2X7R^+$ and $P2X7R^-$ fractions of each T cell subset were analyzed separately for (**B**) ADP-ribosylation by total eNAD staining and (**C**) NICD based on co-staining with eNAD and DAPI. Repeated measures one-way ANOVA was used to determine statistically significant differences between treatments. Each connected line represents paired analysis of one mouse. Bars indicate mean values. The experiment was performed three times with similar results. Percentage data were square root-transformed prior to statistical testing. ns, not significant; *p<0.05, **p<0.01. ***p<0.001, ****p<0.0001

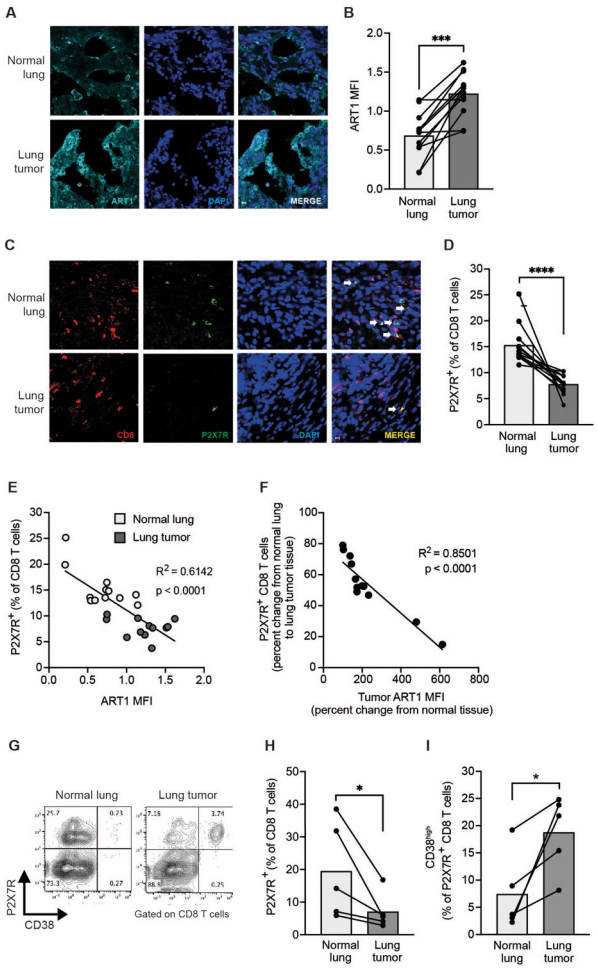

Figure 5. ART1 overexpression in human lung tumors is associated with low infiltration of P2X7R$^+$ CD8 T cells.

(**A to F**) Analysis of immunofluorescence stainings of lung tumor tissue and matched normal lung tissue from patients with lung adenocarcinoma (n=12). (**A**) Representative images of ART1 immunofluorescence staining in lung tumor and matched normal tissue are shown. Scale bar indicates 10 μm. (**B**) The bar graph depicts mean fluorescence intensity (MFI) of ART1 staining normalized to the MFI of Hoechst in lung tumor and matched normal tissue. Data were analyzed by a paired t-test. (**C**) Representative images of CD8 (red), P2X7R (green) and nuclear stain by Hoechst (blue) are shown for lung tumor and matched normal tissue. Yellow color in the merged images indicate co-localization of CD8 and P2X7R staining (highlighted by white arrows). Scale bar indicates 10 μm. (**D**) The bar graph depicts the percentage of P2X7R$^+$ CD8 T cells among CD8 T cells in lung tumor and matched normal tissue. Data were analyzed by a paired t-test. (**E**) Linear regression analysis correlating frequency of P2X7R$^+$ CD8 T cells among total CD8 T cells with ART1 MFI is shown. Light gray circles represent normal tissue. Dark gray circles represent lung tumor tissue. (**F**) Linear regression analysis shows the correlation between percent change of P2X7R$^+$ CD8 T cells in lung tumor tissue from matched normal tissue with percent change in ART1 MFI of lung tumor tissue from matched normal tissue. R^2 represents the Pearson correlation coefficient. (**G to I**) Flow cytometry was used to characterize CD8 T cells

infiltrating lung tumor tissue and adjacent matched normal lung tissue from patients with lung adenocarcinoma (n=5). (**G**) Representative dot plots of P2X7R and CD38 expression on CD8 T cells infiltrating normal lung tissue and lung tumor tissue are shown. (**H**) The percentage of CD8 T cells expressing P2X7R is shown. Data were analyzed by a paired t-test. (**I**) The percentage of $P2X7R^+$ CD8 T cells with high surface expression of CD38 is shown. Data in (H and I) were analyzed by a paired t-test. Bars graphs in (B, D, H, and I) indicate mean values. Percentage and MFI data were log-transformed prior to statistical testing. *p<0.05, ***p<0.001, ****p<0.0001.